# PHOTOCATALYTIC PROPERTIES OF SILVER LOADED TITANIUM DIOXIDE POWDERS PRODUCED BY MECHANICAL BALL MILLING

A THESIS SUBMITTED TO
THE GRADUATE SCHOOL OF NATURAL AND APPLIED SCIENCES
OF
MIDDLE EAST TECHNICAL UNIVERSITY

BY

BAŞAK AYSİN

IN PARTIAL FULFILLMENT OF THE REQUIREMENTS
FOR
THE DEGREE OF MASTER OF SCIENCE
IN
METALLURGICAL AND MATERIALS ENGINEERING

FEBRUARY 2012

Approval of the thesis:

# PHOTOCATALYTIC PROPERTIES OF SILVER LOADED TITANIUM DIOXIDE POWDERS PRODUCED BY MECHANICAL BALL MILLING

submitted by **BAŞAK AYSİN** in partial fulfillment of the requirements for the degree of **Master of Science in Metallurgical and Materials Engineering Department, Middle East Technical University** by,

Prof. Dr. Canan Özgen ______________________
Dean, Graduate School of **Natural and Applied Sciences**

Prof. Dr. Tayfur Öztürk ______________________
Head of Department, **Metallurgical and Materials Engineering**

Prof. Dr. Abdullah Öztürk ______________________
Supervisor, **Metallurgical and Materials Eng. Dept., METU**

Assist. Prof. Dr. Jongee Park ______________________
Co-Supervisor, **Metallurgical and Materials Eng. Dept., Atılım University**

**Examining Committee Members:**

Assoc. Prof. Dr. Caner Durucan ______________________
Metallurgical and Materials Engineering Dept., METU

Prof. Dr. Abdullah Öztürk ______________________
Metallurgical and Materials Engineering Dept., METU

Assist. Prof. Dr. Jongee Park ______________________
Metallurgical and Materials Engineering Dept., Atılım University

Assist. Prof. Dr. H.Emrah Ünalan ______________________
Metallurgical and Materials Engineering Dept., METU

Prof. Dr. Gürkan Karakaş ______________________
Chemical Engineering Dept., METU

**Date:** *09.02.2012*

**I hereby declare that all information in this document has been obtained and presented in accordance with academic rules and ethical conduct. I also declare that, as required by these rules and conduct, I have fully cited and referenced all material and results that are not original to this work.**

Name, Last name : Başak Aysin

Signature :

# ABSTRACT

## PHOTOCATALYTIC PROPERTIES OF SILVER LOADED TITANIUM DIOXIDE POWDERS PRODUCED BY MECHANICAL BALL MILLING

AYSİN, Başak
M.Sc., Department of Metallurgical and Materials Engineering
Supervisor: Prof. Dr. Abdullah ÖZTÜRK
Co-Supervisor: Assist. Prof. Dr. Jongee PARK

FEBRUARY 2012, 89 pages

Silver (Ag) was loaded to three different kinds (P-25, NT-22, and $TiO(OH)_2$) of titanium dioxide ($TiO_2$) powders through adding three different quantities (4.6, 9.2, and 13.8 ml) of silver nitrate ($AgNO_3$) solution by mechanical ball milling process. X-Ray diffraction analysis suggested that Ag was loaded on the $TiO_2$ powders in the form of silver oxide (AgO). SEM, particle size, and BET surface area analyses revealed that $TiO_2$ particles agglomerated after ball milling, resulting in the decrease of specific surface area of the $TiO_2$ powders. Powders P-25, NT-22, and $TiO(OH)_2$ degraded 94 %, 46 %, and 26 %, respectively of MO solution under 1 h UV irradiation. Increasing amount of Ag loading enhanced photocatalytic activity of $TiO_2$ powders under UV irradiation. The best photocatalytic performance was achieved by 13.8 ml $AgNO_3$ solution added NT-22 powders. Percent methyl orange (MO) degradation of 13.8 ml $AgNO_3$ solution added P-25, NT-22, and $TiO(OH)_2$ powders under 1 h UV irradiation was 85 %, 96 %, and 67 %, respectively. Contact angle measurements revealed that hydrophilic properties of $TiO_2$ powders were also improved by Ag loading. Moreover, $TiO_2$ powders gained antibacterial prospect after Ag addition. Ag loaded

$TiO_2$ powders could be used effectively for the applications requiring better photocatalytic activity and antibacterial effect.

**Keywords: photocatalysis; titanium dioxide; silver; ball milling; methyl orange solution**

# ÖZ

## MEKANİK BİLYALI ÖĞÜTMEYLE ÜRETİLMİŞ GÜMÜŞ YÜKLENMİŞ TİTANYUM OKSİT TOZLARININ FOTOKATALİTİK ÖZELLİKLERİ

AYSİN, Başak
Yüksek Lisans, Metalurji ve Malzeme Mühendisliği Bölümü
Tez Yöneticisi: Prof. Dr. Abdullah ÖZTÜRK
Ortak Tez Yöneticisi: Yard. Doç. Dr. Jongee PARK

Şubat 2012, 89 sayfa

Mekanik bilyalı öğütme yöntemi ile üç farklı $TiO_2$ (P-25, NT-22, and $TiO(OH)_2$) tozuna üç farklı miktarda (4.6, 9.2, and 13.8 ml) $AgNO_3$ solüsyonu kullanılarak gümüş yüklenmiştir. X-Ray kırılınım analizi gümüşün $TiO_2$ tozlarına AgO formunda yüklendiğini göstermiştir. SEM, parçacık boyut analizi ve BET yüzey alanı analizleri $TiO_2$ parçacıklarının bilyalı öğütmeden sonra aglomare olduğunu, bunun sonucunda da $TiO_2$ tozlarının spesifik yüzey alanlarının azaldığını ortaya koymuştur. P-25, NT-22 ve $TiO(OH)_2$ tozları 1 saat UV ışıması altında MO solüsyonunu sırasıyla % 94, % 46 ve % 26 bozunmaya uğratmışlardır. Artan Ag yüklemeleri $TiO_2$ tozlarının UV ışınımı altındaki fotokatalitik aktivitesini arttırmıştır. En iyi fotokatalitik performans 13.8 ml $AgNO_3$ solüsyonu eklenen NT-22 tozları ile elde edilmiştir. 13.8 ml $AgNO_3$ solüsyonu eklenen P-25, NT-22 ve $TiO(OH)_2$ tozları 1 saat UV ışınımı altında MO solüsyonunu sırasıyla % 85, % 96 ve % 67 bozunuma uğratmıştır. Temas açısı ölçümleri ise $TiO_2$ tozlarının hidrofilik özelliklerinin Ag eklenerek iyileştirildiğini ortaya koymuştur. Bunun yanı sıra, $TiO_2$ tozları Ag eklenmesinden sonra antbakteriyel özellik de kazanmışlardır. Ag yüklenmiş $TiO_2$ tozları fotokatalitik ve antibakteriyel özellik gerektiren uygulamalarda etkili bir şekilde kullanılabilirler.

**Anahtar Kelimeler: fotokataliz; titanyum dioksit; gümüş; bilyalı değirmen; metil turuncusu solüsyonu**

*To my family*

# ACKNOWLEDGEMENTS

I would like to express my deepest gratitude to my supervisor Prof. Dr. Abdullah Öztürk, for his endless support, advice, encouragement, and patience. Without him, this thesis would not be done.

I would also like to thank to Assist. Prof. Dr. Jongee Park for his guidance throughout all the experiments.

I wish to give my special thanks to my friend for long years, Ayşegül Afal, METU and METE would be very different without you. I also wish to thank my laboratory partner Esra Çorapçı for being such a good friend, the best things happen when you have no expectation.

I want to thank to my friends from E-Building Derya, Volkan, Metehan, Fuat, Ebru, Şerif, Berk, Nursev and Eylem for making our work enviroment such a unique place. I also thank to Barış Özdemir, Şahin Coşkun, Evren Tan and Güher Kotan for their support and friendship, and Esen Çevik for his technical support and guidance.

I want to thank to our staff from the department, especially to Necmi Avcı and Saffet Ayık, METU Central Laboratory and METU Medical Center for their help during my studies.

I especially thank to my dearest friends Çağlar Beşiroğlu, Melis Şardan, Ongun Bilgin and Okan Öner Ekiz for their most valuable friendship. This thesis work was easier with their presence in my life.

Financial support of The Scientific and Technological Research Council of Turkey (TÜBİTAK) through the project 109M048 is also acknowledged.

Finally, I want to thank to my parents who always believed in me. Without their love, support and trust, this thesis would not be done.

# TABLE OF CONTENTS

# LIST OF TABLES

# LIST OF FIGURES

# CHAPTER 1

# INTRODUCTION

In today's world, environmental issues are one of the biggest concerns of the industry. Pollution of air and water due to consumption of fossil fuels or emission of chemical substances is a global problem (Taoda, 2008). The photocatalysis concept has been studied for the last fifty years in order to prevent the damages of the pollution from the organic substances (Heller, 1981). The use of semiconductor titanium dioxide ($TiO_2$) has drawn attention for photocatalytic applications since it is highly photostable and low polluting (Gadalla et al., 2009; Su et al., 2004). Also, it is easily available in the market, cheap and non toxic.

$TiO_2$ based photocatalysts are still the most commercialized products in the market although there are different alternatives present. They are widely used in different areas such as bactericidal and water purification applications. Some of the major applications of $TiO_2$ photocatalyst are shown in Figure 1.1. $TiO_2$ photocatalyst is considered to be used for several other applications such as water disinfection, determination of dissolved organic nitrogen compounds in natural waters, photoreduction of mercuric salt solutions (Jacoby et al. 1998; Lau et al., 1998). Some of the $TiO_2$-based photocatalytic products that have appeared in the market in Japan are shown in Table 1.1.

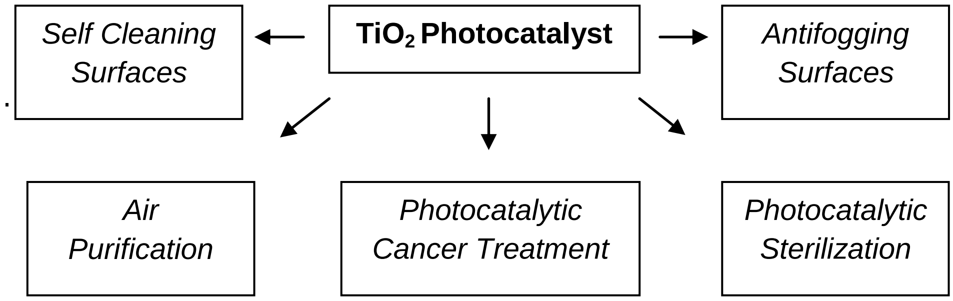

**Figure 1.1** Major applications where $TiO_2$ photocatalyst used (Fujishima et al., 2000).

**Table 1.1.** $TiO_2$-based photocatalytic products that have appeared in the market in Japan ( Fujishima and Zhang, 2006).

| Categories | Products | Properties |
|---|---|---|
| Exterior construction materials | Tiles, glass, tents, plastic films, aluminum panels, coatings | Self cleaning |
| Interior furnishing materials | Tiles, wallpaper, window blinds | Self cleaning, antibacterial |
| Road-construction materials | Soundproof & tunnel walls, road blocks, coatings, traffic sign lamp covers | Self cleaning, air cleaning |
| Purification facilities | Air cleaners, air conditioners, purification system for pools | Air / water-cleaning, antibacterial |
| Household goods | Fibers, clothes, leathers, lightings, sprays | Self cleaning, antibacterial |
| Others | Facilities for agricultural uses | Air cleaning, antibacterial |

Studies in order to improve the photocatalytic efficiency of these products are still vital both for industry and scientists due to the fact that $TiO_2$ is a wide band photocatalyst. It has a physical limitation of having a large band gap for wide range of applications (Konta et al., 2004). Efforts continue to decrease band gap energy and hence to improve the photocatalytic activity of $TiO_2$ powders. In that regard, different production techniques such as sol-gel processing, hydrothermal processing, ball milling (Kim et al., 2004; Kim, 2006; Ovenstone, 2001; Sonawan et al., 2003) or different modifications such as dopant addition with metals like silver (Ag), vanadium (V), iron (Fe), gold (Au) and platinum (Pt) (Zaleska, 2008), non metals like nitrogen (N), sulphur (S), carbon (C), boron (B) and phosphorus (P) (Zaleska, 2008) or coupling with other semiconductors like tin oxide ($SnO_2$) or zinc oxide (ZnO) (Kumar and Devi, 2011) have been tried. In spite of some studies reported on Ag loading on $TiO_2$ particles or films by photochemical deposition (Lee et al., 1993), by chemical reduction method (Priya et al., 2009), by hydrothermal method (Liu et al., 2003), by sol-gel process (Akgun et al., 2011a; Ghanbary and Jafarian, 2011) or by laser induction (Whang et al., 2009), Ag loading on $TiO_2$ particles by ball milling has not been studied yet.

The objective of this study was to improve photocatalytic activity of $TiO_2$ particles by Ag loading via mechanical process of ball milling. Ag was selected as modification agent since it improves photocatalytic properties of $TiO_2$ (Lee et al., 1993; Scalafani et al.,1991) and also provides antibacterial activity to $TiO_2$ (Akgun et al., 2011a; Whang et al., 2009). A planetary type ball mill was employed for the simultaneous size reduction and Ag loading to $TiO_2$ particles since it is relatively simple and highly versatile. Powders produced were characterized through X-Ray powder diffraction (XRD), Scanning Electron Microscope (SEM), Particle size analysis and Brunauer-Emmett-Teller (BET) surface analysis. Photocatalytic activity of powders was investigated by means of methyl orange (MO) degradation under ultraviolet (UV) irradiation. Hydrophilicity of the powders was determined by contact angle measurement. Also, basic antibacterial activity measurements were performed to see whether Ag loading brings any antibacterial prospect on the $TiO_2$ powders produced.

# CHAPTER 2

# LITERATURE REVIEW

## 2.1. PHOTOCATALYSIS

Environmental problems related to hazardous wastes, contaminated ground waters or toxic air contaminants are among the prior concerns for nations in recent years. In order to eliminate or minimize the hazardous compounds of these wastes, advanced physicochemical methods such as semiconductor photocatalysis have been developed (Hoffmann et al., 1995). The photocatalysis subject is being studied for 50 years now, and the term photocatalysis is still being argued. It is argued that photocatalyzed reaction implies that the light is the catalyst; although, light is a reactant consumed through the chemical process. The term photocatalysis is actually defined as “ acceleration of photoreaction by the presence of a photocatalyst” (Mills and Hunte, 2000). Photoinduced molecular transformation or reaction occurs at the surface of a catalyst. After the initial excitation, system is followed by a subsequent electron and/or energy transfer (Linsebigler et al., 1995).

The basic theory for a photocatalytic reaction depends on the illumination with photons. When the photons energy is equal to or greater than the band gap energy $E_G$ ($h\nu \geq E_G$) of a photocatalyst, the absorption of photons leads to the formation of electron-hole pairs within the bulk (Herrmann, 2006). By the help of reemitted energy as light or heat, recombination of these charge carriers or their migration to catalyst surface in order to participate in redox reactions at the interface is possible (Byrne et al., 2011). There is an adequate lifetime for electron hole pairs to undergo charge transfer after the excitation across the band gap. The process is called as heterogeneous photocatalysis if the semiconductor remains intact while the charge transfer for adsorbed species is continuous and exothermic (Linsebigler et al., 1995). Schematic illustration of photoexcitation in a solid followed by deexcitation events is shown in Figure 2.1.1.

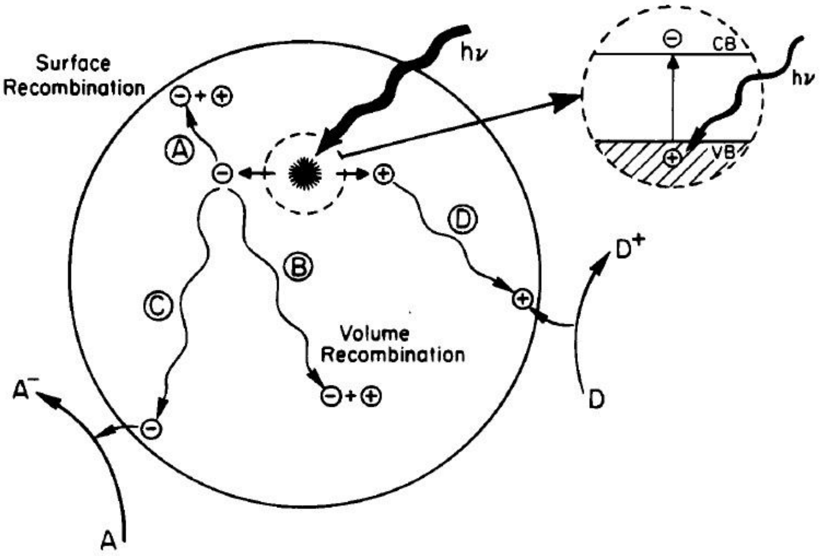

**Figure 2.1.1.** Photoexcitation in a solid followed by deexcitation events (Linsebigler et al., 1995).

The migration of electrons and holes to semiconductor surface causes the transfer of photoinduced electron to adsorbed species or to the solvents. As the semiconductor donates electrons to reduce an electron acceptor (path C), migration of hole to surface where electron of a donor can combine with surface hole oxidizing donor occurs (path D). Respective positions of the band edges for conduction and valance bands, as well as the redox potential levels of adsorbate species are important factors for probability and rate of charge transfer (Linsebigler et al.,1995).

The overall process can be summarized by the following equation (Mills and Hunte, 2000);

$$A+D \xrightarrow[E_{Light} \geq E_{bg}]{\text{Semiconductor}} A^{-} + D^{+}$$

A= Acceptor

D= Donor

$E_{bg}$= Band gap energy of semiconductor

The reactive oxygen species produced by these reactions are very active; they can destroy chemical contaminants in water and can also cause an important amount of damage to microorganism. Carbon dioxide ($CO_2$), water ($H_2O$) and inorganic acids or salts are the final products of the reaction (Byrne et al., 2011).

There are several semiconductor materials used for photocatalytic applications. Some of the commonly used semiconductors are given in Table 2.1.1.

**Table 2.1.1.** Widely used semiconductors, their band gap and wavelength (Ersöz, 2009).

| ***Semiconductor*** | ***Band Gap (eV)*** | ***Wavelength (λ-nm)*** |
|---|---|---|
| $TiO_2$ (Anatase) | 3.2 | 388 |
| $TiO_2$ (Rutile) | 3.0 | 413 |
| $SnO_2$ | 3.6 | 338 |
| ZnO | 3.4 | 363 |
| $Fe_2O_3$ | 2.3 | 539 |

Being chemically and biologically inert, stable to corrosion and non toxic, $TiO_2$ is the most widely used semiconductor for environment applications and has been studied extensively for photocatalytic degradation of harmful organic compounds (Hong et al., 2005). On the other hand, it has some drawbacks limiting the application areas. Wide band gap (3.2 eV) of $TiO_2$, which corresponds to a wavelength less than 390 nm, causes the material to utilize only 3-4% of solar energy reaching to earth (Rattanakam and Supothina, 2009).

## 2.2. TITANIUM DIOXIDE PHOTOCATALYST

$TiO_2$ has became a material for photocatalysis on photoelectrochemical solar conversion, environmental photocatalysis like self cleaning surfaces or photoinduced hydrophilicity involving antifogging and self cleaning properties. Although the types of photochemistry for photocatalysis and hydrophilicity are different, both takes place on the same surface made from $TiO_2$ photocatalyst (Fujishima et al., 2000).

Availability of the material is one of the most important issues for environmental photocatalysis. Being relatively inexpensive, having high chemical stability and having highly oxidizing photogenerated holes which are also reducing enough for production of superoxide from dioxygen are some of the other aspects for choosing $TiO_2$ as a material for photocatalysis (Byrne et al., 2011). Schematic representation of the mechanism of photocatalysis on $TiO_2$ particle is illustrated in Figure 2.2.1.

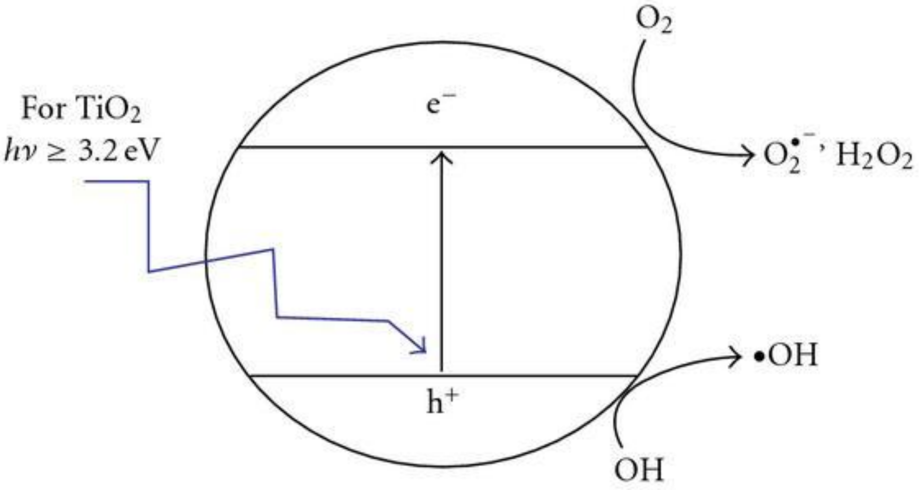

**Figure 2.2.1.** Schematic representation of the mechanism of photocatalysis on $TiO_2$ particles (Byrne et al., 2011).

$TiO_2$ has three crystal structures; rutile, anatase or brookite. Brookite structure is more compact than anatase; but, less compact than rutile (Yin et al., 2003). Anatase and rutile both having distorted octahedron class crystal structure are widely used in photocatalysis, while researchs report that it is difficult to prepare brookite without any anatase or rutile phase limiting its study and application (Dipaola et al., 2007; Xie et al. 2009). For rutile crystal structure, a slight distortion from orthorhombic structure occurs, while for anatase crystal structure the distortion of cubic lattice is noteworthy causing a less orthorhombic symmetry (El et al., 2011; Thompson and Yates, 2006). The schematic representation of crystal structures for anatase and rutile phases of $TiO_2$ is shown in Figure 2.2.2.

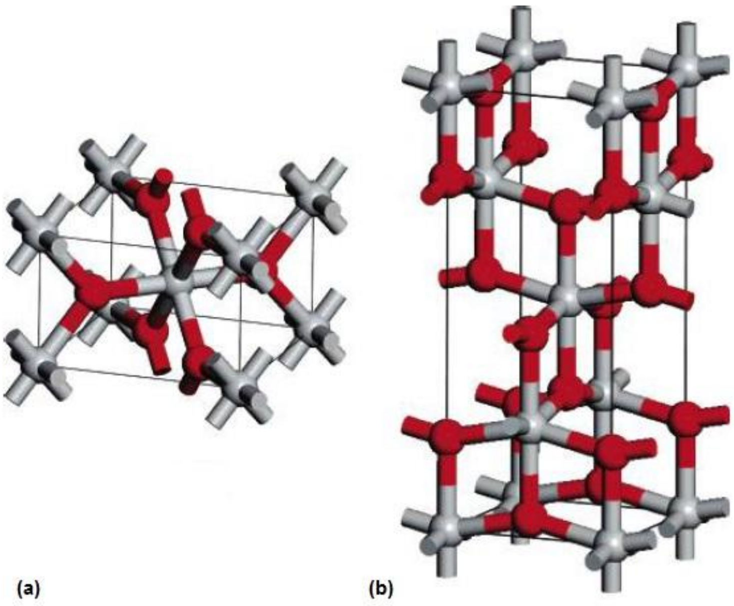

**Figure 2.2.2.** Schematic representation of the crystal structures of $TiO_2$ **(a)** Rutile, **(b)** Anatase. Gray atoms are titanium and red atoms are oxygen (Thompson and Yates, 2006).

Rutile has lower band gap energy (3.0 eV) than anatase (3.2 eV) (Ersöz, 2009). Although rutile is expected to have better photocatalytic properties than anatase due to its lower band gap, anatase is more active than rutile because of the fact that rutile has larger crystal size (El Saliby et al., 2011). Mixture of anatase and rutile catalysts possessed a significantly higher photocatalytic activity than the pure phases. Degussa P-25, a standard industrial photocatalyst with a composition of 70% anatase and 30% rutile, is an example for this behavior. The main reason is attributed to better charge carrier separation in the mixed phase (Sun et al., 2003).

Larger surface area is desirable for better photocatalytic performance since photocatalytic reaction occurs on the catalyst surface. Surface area of $TiO_2$ photocatalyst can be increased by different methods to improve its photocatalytic activity.

Majority of research done on $TiO_2$ materials are based on the band gap modification, mainly decreasing the energy required for excitation for the utilization of a larger fraction of visible light. With the band gap of 3.0-3.2 eV, $TiO_2$ materials have a threshold extending from the ultraviolet region into the solar spectrum to about 400 nm. The threshold energy for photoactivation can be reduced by doping $TiO_2$ with metals or non-metals. A reduction in threshold energy for photoactivation leads a potential increase in photoactivity even under solar irradiation (Thompson and Yates, 2006).

## 2.3. WAYS TO IMPROVE THE PHOTOCATALYTIC ACTIVITY OF $TiO_2$

### 2.3.1. Particle Size Reduction

Production of small size particles are of interest for new material synthesis since fine particles are processed at lower temperatures, have high catalytic activity and better mechanical properties in comparison to large particles (Jang et al., 2001). Particle size is an important factor on photocatalytic activity. The smaller the particle size, the larger the specific surface area and hence better the photocatalytic activity since photoinduced reaction occurs at the surface of the catalyst in a photocatalytic reaction. When a photocatalyst is illuminated with a stronger light than its band gap energy, diffusion of electron-hole pairs to surface of the catalyst takes place and these electron hole pairs participates in the chemical reaction. The number of active surface sites increases by smaller particle size leading an increase on the surface charge carrier transfer rate (Jang et al., 2001; Zhang et al., 1998).

There are several methods to produce fine photocatalyst particles including sol-gel process (Li et al., 2002; Nolan, 2010; Su et al., 2004), hydrothermal process (Inagaki, 2001; Lu et al., 2008; Ovenstone, 2001) or mechanical methods like ball milling (Fadhel et al., 1999; Gajovic, 2001; Yin, 2006; Zhang et al., 2008). Brief information about each process is given in the following subsections.

#### *2.3.1.1. Sol-Gel Process*

Sol-gel is one of the most widely used process for the production of nanosized materials with high photocatalytic activities (Su et al., 2004). $TiO_2$ is prepared by reactions of hydrolysis and polycondensation of titanium alkoxides to form oxopolymers transforming into an oxide network. The reaction scheme is as follows (Su et al., 2004);

1. Hydrolysis

$$M(OR)_n + H_2O \longrightarrow M(OR)_{n-1}(OH) + ROH$$

2. Condensation

Dehydration

$$M(OR)_n + M(OR)_{n-1}(OH) \longrightarrow M_2O(OR)_{2n-2} + ROH$$

Dealcoholation

$$2M(OR)_{n-1}(OH) \longrightarrow M_2O(OR)_{2n-2} + H_2O$$

Overall reaction

$$M(OR)_n + \frac{n}{2}\, H2O \longrightarrow MO_{n/2} + {}_nROH$$

Sol-gel method has the advantages like low processing temperature and good homogeneity; but, it also has disadvantages such as complex chemisty of the process or expensive chemical products like the organic solvents (Han et al., 2010; S. Hong, 2003; Niederberger and Pinna, 2009).

#### *2.3.1.2. Hydrothermal Process*

For the preparation of different inorganic materials in nanocrystalline state, hydrothermal synthesis is a widely used method (Zhu et al., 2004). Since the reactions are carried out in an enclosed system, the method using an aqueous solvent as reaction medium can be classified as environmentally friendly. The presence of different mineralizers like hydroxides or fluorides of alkalis at different pH values of usage of distilled water during the hydrothermal treatment of $TiO_2.nH_2O$ amorphous gels is an important aspect for the hydrothermal synthesis of nanocrystalline titania (Kolen’ko et al., 2004). Titanium alkoxide and alcohol are generally used as precursor solution for the preparation of nanocrystalline $TiO_2$ powders via hydrothermal method. Acid and organic additives are also added into the solution in order to induce crystallization and prevent particle agglomeration (Bao et al., 2005).

Hydrothermal method provides excellent homogeneity and possibility of deriving unique stable structures at low reaction temperatures. However, the method also requires further heat treatment and repeated washing to remove organic solvent and additives (Bao et al., 2005; Nam and Han, 2003).

#### *2.3.1.3. Ball Milling*

Ball milling is an efficient and simple method for the fabrication of sub-micron or nanostructured powders. It is widely used for the production of nanocrystalline materials. During the ball milling process, the elastic and plastic deformation of powders between balls and wall of the jar under high energy is observed. In ball milling process three simultaneous events occur which are cold-welding, fracturing and annealing of powder grains (Dutta et al., 2002). Mechanical alloying by ball milling is a complex process due to the dependence of the process on many factors such as type of mill, milling dynamical conditions, temperature, chemical composition of powder mixture and properties of grinding tools (Begin-Colin et al., 2000).

Basic mechanisms of milling still remains as an uncleared issue; although, plenty of theoretical models are studied to explain the physics of milling process in order to predict the end product of final milling. High energy ball mill usually causes several mechanochemical phase transitions during ceramic powder processing (Dutta et al., 2002). Furthermore, final products of milling can be composed of different phases along with contaminations coming from the milling media. During ball milling process, an equilibrium between breakage and rewelding of powders can occur and this can cause the unalteration of particle size on further milling due to agglomeration of smaller particles (Dutta et al., 2002).

There are different types of ball milling techniques based on the movement of milling balls and vial, such as vibration mill, planetary mill and attritor (Zhang et al., 2008). A schematic illustration of the planetary ball mill is given in Figure 2.3.1. Planetary ball mill takes its name from the planet-like movement of the vials. Vials on a rotating supporting disk are also rotated around their axes by a special drive mechanism. The centrifugal force produced by the vials rotating around their own axes and that produced by the rotating support disk both act on the vial contents. The opposite rotation of vials and rotate disk causes centrifugal forces to act in opposite directions also leading the balls to run down inside the vial, called as friction effect, and the grinding of the material. When grinding balls lift off and travel freely through the inner chamber of the vial, they collide against the opposing inside wall, called as the impact effect (Castro and Mitchell, 2002).

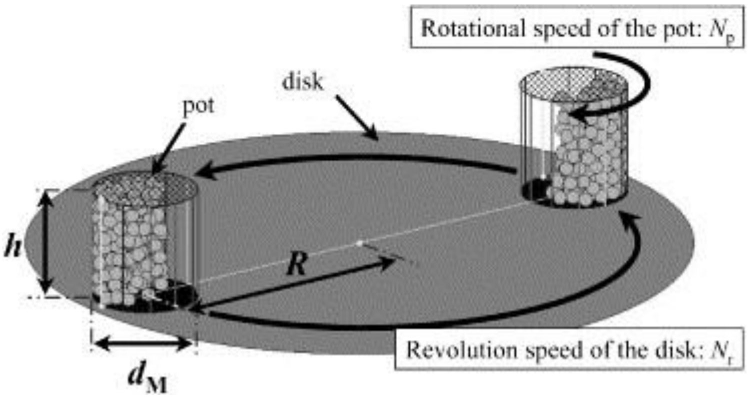

**Figure 2.3.1.** Schematic illustration of the planetary ball mill (Mio et al., 2004).

Using planetary ball mill for the particle size reduction of $TiO_2$ photocatalyst is a common method for nanocrystalline powder production since it is relatively simple and highly versatile (Salari et al., 2009). Starting material used for the production of nanocrystalline powder changes in a wide range from micron sized powders to precursors.

In this study, ball milling is chosen for particle size reduction and dopant addition. All the results throughout the study were obtained by means of a planetary ball mill.

### 2.3.2. Dopant Addition

In a reactive semiconductor substrate, energy levels for electron transfer between adsorbate molecules can be provided by the catalyst while the catalyst can also behave as an electron donor (as the photogenerated electron in conduction band) and as an electron acceptor (photogenerated hole in valence band). The band structure of the substrate is vital since a change in surface or bulk electronic structure can affect the chemical events (Linsebigler et al., 1995). Semiconductor band gap structure is shown schematically in Figure 2.3.2.

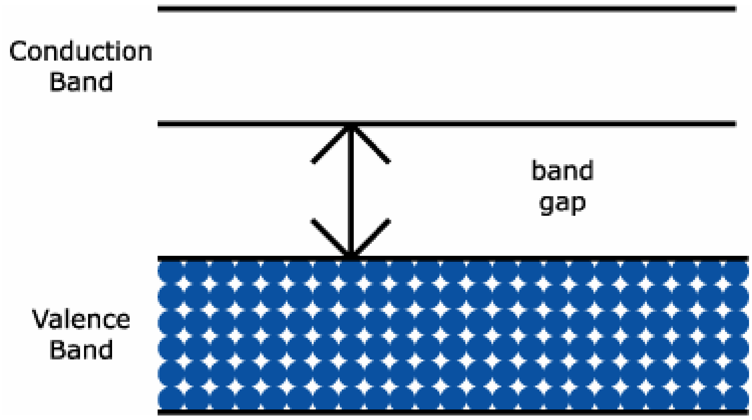

**Figure 2.3.2.** Semiconductor Band Gap Structure (Algarin, 2008).

$TiO_2$ being a wide band gap semiconductor requires light below 388 nm to create an electron–hole pair. Use of $TiO_2$ can be extended for solar light applications by shifting the band gap into the range of visible light (Hong et al., 2005). Inducing dopants into $TiO_2$ have been widely studied to shift into the visible part of spectrum as well as improving the photoefficiency of the electronic process. Trapping an electron or hole alone is inefficient, since immobilized charge species quickly recombine with the mobile counterpart (Colón et al., 2006). Metal ions serving as charge trapping sites and interceding in the interfacial transfer improves photoefficiency by reducing electron-hole recombinaton rates. Effect of transition metal on photocatalytic activity depends on many factors such as method of doping, type of the dopant and the concentration of the dopant (Colón et al., 2006).

$TiO_2$ was modified with many different metals and nonmetals as stated in Chapter 1. Fe, one of the most used metal dopant addition, was added into $TiO_2$ with different methods like mechanochemical alloying, sol-gel process or ultrasonic method (Han et al., 2008; Hung et al., 2007; Kim et al., 2004; Zhou et al., 2006), Cu, another common metal, was doped with methods like sol-gel or mechanical alloying (Colón et al., 2006; Park et al., 2006), and Ag using different methods like photoreduction treatment, sol-gel process or liquid impregnation method (Arabatzis et al., 2003; Sahoo et al., 2005; Wodka et al., 2010). Non metals C or N were also doped into $TiO_2$ with various methods such as ball milling or sol-gel process (Yin, 2006; Wu et al., 2010).

In this study, Ag loading was chosen to modify $TiO_2$. Information on Ag loading is given in the following section.

#### *2.3.2.1. Ag Doping*

Regardless of its form (bulk or finely dispersed), metallic silver (Ag) is an important material for many technologies. It has useful properties such as chemical stability, electrical and thermal conductivity, catalytic activity, antibacteriostatic effects and nonlinear optical behavior. As a result Ag nanoparticles are used for catalysts, staining pigments for glasses and ceramics or for antimicrobial applications (Sondi et al., 2003).

In order to improve photocatalytic activity by limiting the recombination reaction, insertion of noble metals has been tried. Especially Ag doping draw attention due to the importance in medical applications of Ag and antibacterial activity of $TiO_2$ together (Seery et al., 2007). Ag doped $TiO_2$ can be used in sanitary wares, medical devices or air conditioning filters.

Ag increases the photocatalytic activity of $TiO_2$ by different mechanisms (Akgun et al., 2011a). It can trap the excited electrons from $TiO_2$ and the holes are left for the degradation reaction of organic species. Extension of wavelength response towards visible region is also observed. Moreover, by creating a local electric field, Ag particles enhance electron excitation.

Some contradictory reports (Akgun et al., 2011a; Seery et al., 2007) note that photocatalytic activity of Ag modified $TiO_2$ decreased due to the following factors;

1. Access of light to $TiO_2$ can be hindered due to high Ag coverage.
2. Active $TiO_2$ sites can be blocked by Ag.
3. Ag can be dispersed poorly.
4. Recombination rates can be increased due to high amount of doping than optimal amount.
5. Role of $O_2$ can be inhibited due to scavenging of electrons by Ag deposits.

There are several methods used for Ag addition to $TiO_2$ materials. $AgNO_3$ is the common Ag source for many studies. Some amount of $AgNO_3$ is added into distilled water or ethanol to prepare $AgNO_3$ solution. Then this solution is either added to powder slurries or precursor solutions of $TiO_2$ to obtain Ag-$TiO_2$ materials via sol-gel and photodecomposition methods (Bowering et al., 2007; Kondo and Jardim, 1991; Liga et al., 2010; Xin et al., 2005). In this study, $AgNO_3$ was used as the Ag source and added to $TiO_2$ by employing a planetary ball mill to obtain Ag loaded $TiO_2$ powder.

# CHAPTER 3

# EXPERIMENTAL PROCEDURE

## 3.1. POWDER PREPARATION

Three different commercial $TiO_2$ powders were used as the starting material. Anatase $TiO_2$ powders (NT-22) and $TiO(OH)_2$, known as metatitanate, were received from Nano Co. Anatase and rutile containing well known $TiO_2$ powders (P-25) was received from Degussa. All three powders were used without any additional purification process. Selected properties of starting $TiO_2$ powders as quoted by their manufacturers are listed in Table 3.1.1. Silver nitrate ($AgNO_3$) received from Merck and sodium carbonate ($Na_2CO_3$) supplied from Horasan Kimya were used for Ag loading. Darvan C-N received from Vanderbilt Company Inc. was used as dispersant during milling process.

**Table 3.1.1.** Properties of starting powders

| Property | NT-22 | P-25 | Metatitanate |
|---|---|---|---|
| Formula | $TiO_2$ | $TiO_2$ | $TiO(OH)_2$ |
| Crystalline Phase | Anatase | Anatase and Rutile | Anatase |
| Particle Size (Primary, Secondary) | 15 – 30 nm<br>1 – 2 μm | 21 nm | - |
| $TiO_2$ Content (wt. %) | 98.5 | ≤ 99.5 | - |
| Specific Surface Area ($m^2/g$) | 60-80 | 50 ±15 | - |

A planetary ball mill (PM-100, Retsch) was employed in the basic powder preparation step to obtain dispersed and refined powders. The jar and balls used were made of zirconia in order to obtain better milling without contamination. The volume of the jar was 250 ml and ball diameter was 5 mm. Wet milling was carried out for all milling experiments with distilled water as the wetting media

In order to obtain Ag loaded $TiO_2$ powders, the procedure described by Kondo and Jardim, 1991 was adapted for ball milling. 0.1 M $AgNO_3$ solution and 1% weight/volume (w/v) of $Na_2CO_3$ solution were prepared separately. 10 g of $TiO_2$ powder was poured into 250 ml of zirconia jar containing 50 ml of distilled water. 4.6 ml of the $AgNO_3$ solution prepared and 5 ml of $Na_2CO_3$ solution prepared were added into zirconia jar in given order. The powder to ball ratio used during the experiments was 1:20. Zirconia balls of 5 mm diameter were chosen as milling media with zirconia jar. 2 ml of dispersant was added into the milling solution to avoid agglomeration and reduce wear of jar and balls. Milling was performed at 200 rpm for 1 h continuously without any interval breaks. After milling, the solution was taken out of the jar and poured into a glass beaker. Then the beaker and its content were placed in a dryer at 103 °C for 4 h. After drying is complete, agglomerated powders were ground gently using an agate mortar with pestle. Ground powders were calcined at 400 °C for 1 h in order to remove the organics and to allow the diffusion of the loaded material.

The flowchart of the experimental procedure for the Ag loading on $TiO_2$ powders is shown Figure 3.1.1. The experimental procedure was repeated for 9.2 ml $AgNO_3$ and 10 ml $Na_2CO_3$ solutions, and for 13.8 ml $AgNO_3$ and 15 ml $Na_2CO_3$ solutions to observe the effect(s) of Ag loading on the photocatalytic properties of $TiO_2$ powders. Starting powders were also ball milled without Ag addition to see the effects of size reduction and Ag loading independently on photocatalytic properties.

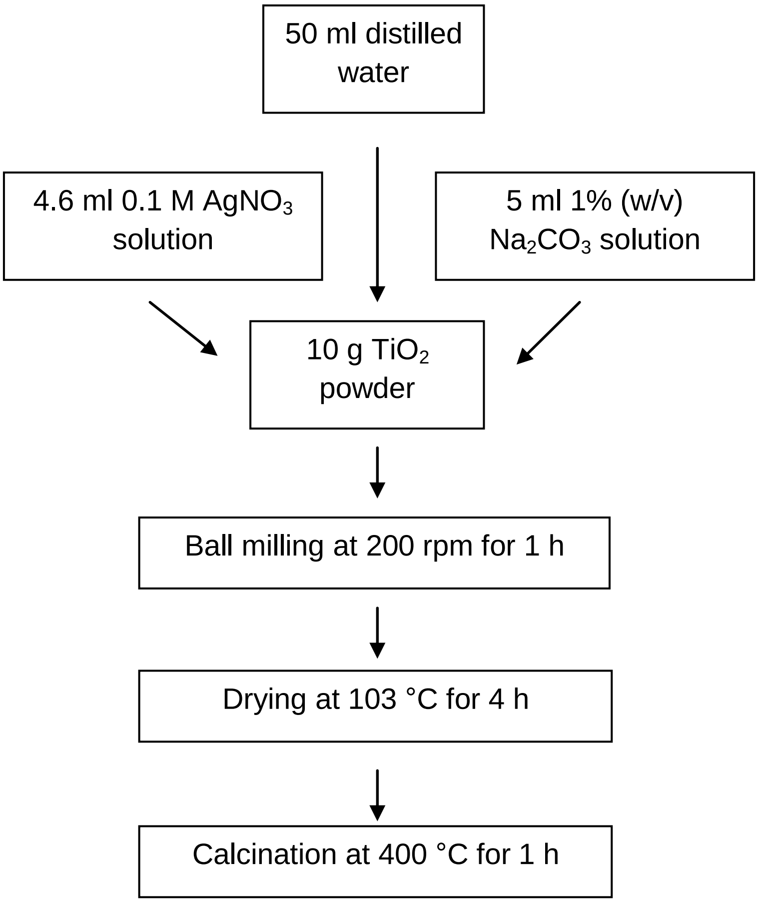

**Figure 3.1.1.** Flowchart of the experimental procedure for Ag loading on $TiO_2$ powders.

## 3.2. CHARACTERIZATION

### 3.2.1. X-ray Diffraction (XRD) Analysis

Powder XRD technique was employed to identify the phases present in $TiO_2$ powders. XRD was also used as experimental criteria for detecting possible zirconia contamination coming from the milling media. The XRD patterns of the $TiO_2$ powders were taken with CuKα radiation by using a Rigaku Geiger-Flex DMAK/B model diffractometer. Each sample was scanned from 2θ of 20º to 80º at a rate of 2º/min by 0.02º increments continuously. For crystallite size calculations, samples were scanned at a rate of 0.5 º/min by 0.02º increments continuously for the characteristic peaks.

### 3.2.2. Scanning Electron Microscope (SEM) and Energy Dispersive Spectroscopy (EDS) Analyses

Scanning electron microscope (Nova NANOSEM 430) was employed to examine surface morphology of the $TiO_2$ powders. Elemental analysis was also performed by EDS to observe presence of Ag and to detect zirconia contamination. In general, specimens are coated with gold (Au) prior to SEM analysis in order to get sufficient conductivity. Instead of Au coating carbon (C) coating was employed before the SEM analysis in this study since Au has overlapping peaks with zirconia.

### 3.2.3. Particle Size Analyses

Particle size analyses were conducted by employing Malvern Mastersizer 2000 and Malvern Zetasizer ZS90 with wet method. For solutions with fully submicron particle size distribution, Malvern Zetasizer was employed while for solutions with micron sized particles Malvern Mastersizer was employed. Solutions taken from ball mill were dispersed with an ultrasonic convertor before analyses.

### 3.2.4. Brunauer-Emmett-Teller (BET) Surface Area Analysis

Surface area of the powders was measured by employing Quantachrome Corporation, Autosorb-6 in by multi point BET method. Before the analysis, powders were preheated for 2 h at 200 °C under vacuum for degassing.

## 3.3. PHOTOCATALYTIC ACTIVITY MEASUREMENT

Photocatalytic activity measurements of the $TiO_2$ powders were carried out in a homemade enclosed box, which provides a fully dark environment without allowing light exposure within the box. A Black-Ray-grade UV semiconductor inspection lamp (100 Watt, 230V~50Hz, 2.0 Amp, 365 nm) and a magnetic stirrer were present inside the box. Scinco S-3100 UV-Vis single beam spectrophotometer was used for the photocatalytic activity measurements.

### 3.3.1. Photocatalytic Activity of $TiO_2$ Powders in Methyl Orange (MO) Solution

Photocatalytic activity of the $TiO_2$ powders was determined using an aqueous MO solution. A 10 mg/L of MO solution was prepared by dissolving 0.01 g of MO powder (Fluka) in 1 L of de-ionized water in a glass beaker. 0.1 g $TiO_2$ powder was added into 100 ml of MO solution. Then, the suspension was placed into the enclosed box. The suspension was stirred continuously at 500 rpm by a magnetic stirrer. For the first 30 min of measurement, the UV light was not turned on, but the suspension was continuously stirred for the powders to absorb MO solution and reach absorption-desorption equilibrium. At the end of first 30 min, 3.5 ml of a sample was taken from the suspension via syringe. Then, by means of syringe filters (Millex Millipore, 0.22 μm) a clear, powder free solution of MO is transferred into quartz cuvette for spectrophotometer measurement. After the first measurement, the UV lamp was turned on and change in absorbance values under UV light were measured in the following 30 and 60 min of the test. The UV exposure time was limited to 60 min. The decreases in absorbance for different samples after 60 min were compared.

The values for percent decrease in absorbance were calculated using the formula;

$$\text{Percent concentration change} = \frac{(Ai-Af)x100}{Ai}$$

Ai = Absorbance value after 30 min without UV light at 467 nm.

A = Absorbance value after 60 min with UV light at 467 nm.

The flowchart of the photocatalytic activity measurement of the $TiO_2$ powders investigated in this study is shown in Figure 3.3.1.

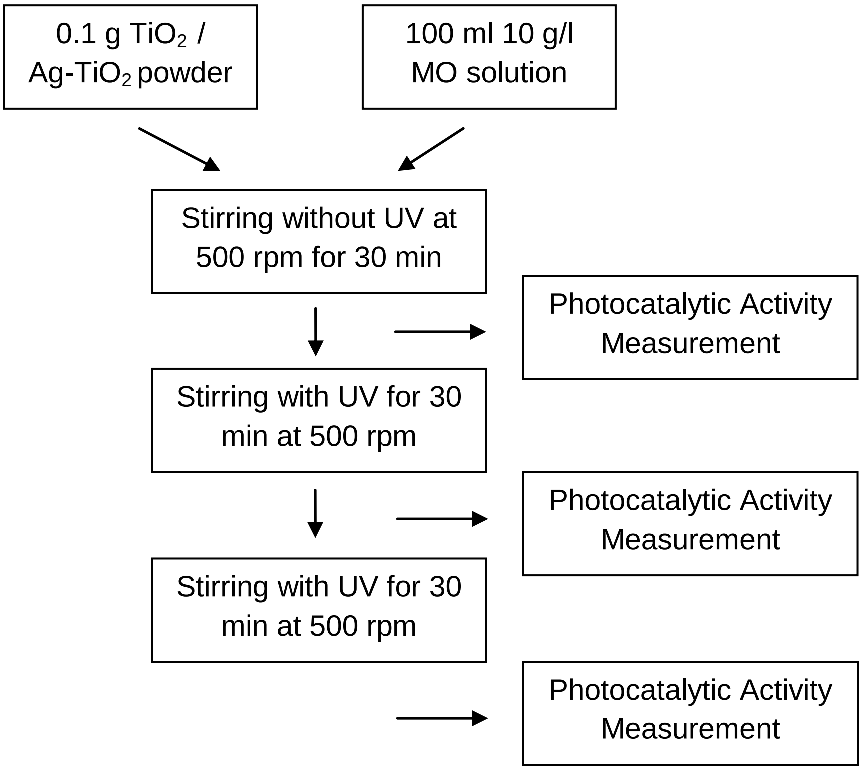

**Figure 3.3.1.** Flowchart showing the photocatalytic activity measurement procedure of the $TiO_2$ powders.

## 3.4. WETTABILITY MEASUREMENT

Wettability of the starting $TiO_2$ powders and Ag loaded $TiO_2$ powders was examined via contact angle measurements. $TiO_2$ powders were coated on glass substrates by dip coating. Before coating, substrates were washed by distilled water and dried. The solution taken from ball mill was used as the coating sol. The substrates were dipped into the solution by hand and dried at room temperature. After drying, substrates were calcined at 350 °C for 1 h. Calcined substrates were taken to Scinco S-3100 UV-VIS single beam spectrophotometer for transmittance measurements. Contact angle of the coated substrates were measured using SEO Phoenix 300 contact angle measurement equipment.

The flowchart for the measurement of the contact angle of $TiO_2$ powders is shown in Figure 3.4.1.

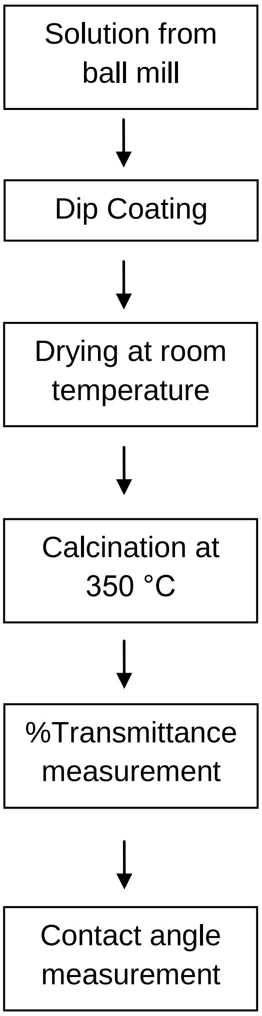

**Figure 3.4.1.** Flowchart showing the contact angle measurement procedure of the $TiO_2$ powders.

## 3.5. ANTIBACTERIAL ACTIVITY TEST

Antibacterial properties of selected starting powders and Ag loaded powders exhibiting the best photocatalytic performance were examined via antibacterial activity tests. Glass substrates (1.25 x 1.25 cm) were coated by a homemade spin coater. Substrates were washed by distilled water and ethanol before coating. After washing, the substrates were dried. The solution taken from ball mill was used as the coating sol. The substrates were placed into the spin coater and coated for 30 s. After coating, substrates were dried at 180 °C. This process is repeated for 5 times to obtain a homogeneous and appropriate coating on the substrate. UV irradiation was not employed in order to see the effect of Ag only. Coated substrates were taken to Medical Center in Middle East Technical University. Agar plates prepared in Medical Center were used as physical seeding for bacteria culture. E.coli bacteria were inserted to agar plates. Coated sides of glass substrates were placed to bacteria containing agar plates and waited for 48 h at 37 °C for incubation. Bare glass substrate without $TiO_2$ coating and P-25 coated glass substrates were also placed into agar as control specimens. The photographs of inhibition zones of substrates were taken for comparison.

The flowchart for antibacterial activity test is shown in Figure 3.5.1.

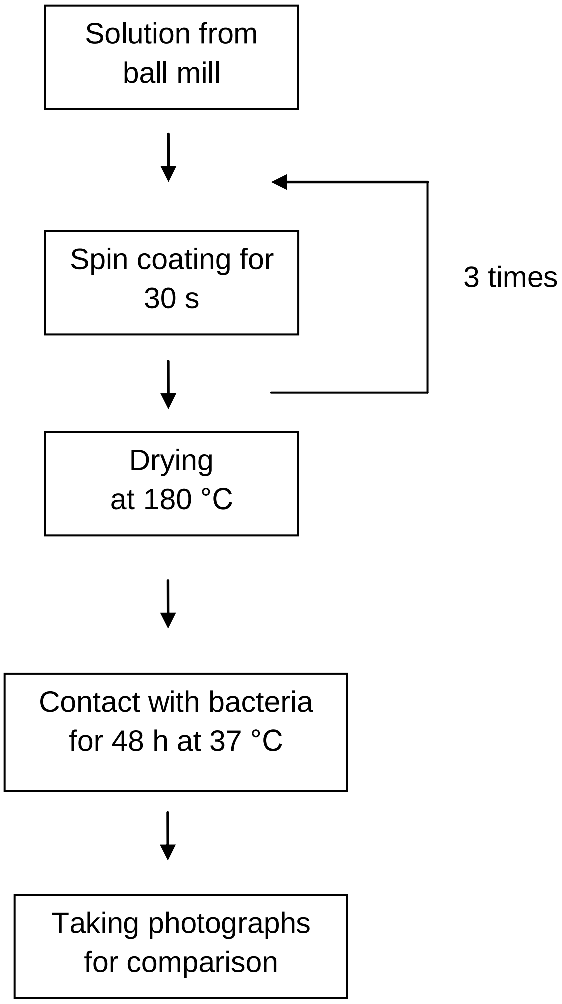

**Figure 3.5.1.** Flowchart showing the steps in antibacterial activity test.

# CHAPTER 4

# RESULTS AND DISCUSSION

## 4.1. GENERAL

In this chapter, results obtained from the experimental studies are presented and discussed.

Three series of $TiO_2$ powders were prepared. “P” series of powders includes starting P-25 powder as obtained, starting P-25 powder as ball milled without Ag addition, and powders produced by adding 4.6, 9.2, and 13.8 ml of 0.1 M $AgNO_3$ solution to starting P-25 powder during milling, are referred to as P, P0, P1, P2, and P3, respectively. “N” series of powders includes starting NT-22 powder as obtained, starting NT-22 powder as ball milled without Ag addition, and powders produced by adding 4.6, 9.2, and 13.8 ml of 0.1 M $AgNO_3$ solution to starting NT-22 powder during milling, which are coded as N, N0, N1, N2, and N3, respectively. “M” series of powders includes starting metatitanate, $TiO(OH)_2$, powder as obtained, starting metatitanate powder as ball milled without Ag addition, and powders produced by adding 4.6, 9.2, and 13.8 ml of 0.1 M $AgNO_3$ solution to starting metatitanate powder during milling, which are coded as M, M0, M1, M2, and M3, respectively. The powders used throughout this study and their code are tabulated in Table 4.1.1. Hereafter, the powders will be referred to as their code unless otherwise is mentioned.

**Table 4.1.1.** The powders used throughout this study and their code.

| Powder | Code |
|---|---|
| P-25 | P |
| Ball milled P-25 | P0 |
| 4.6 ml $AgNO_3$ added P-25 | P1 |
| 9.2 ml $AgNO_3$ added P-25 | P2 |
| 13.8 ml $AgNO_3$ added P-25 | P3 |
| NT-22 | N |
| Ball milled NT-22 | N0 |
| 4.6 ml $AgNO_3$ added NT-22 | N1 |
| 9.2 ml $AgNO_3$ added NT-22 | N2 |
| 13.8 ml $AgNO_3$ added NT-22 | N3 |
| $TiO(OH)_2$ | M |
| Ball milled $TiO(OH)_2$ | M0 |
| 4.6 ml $AgNO_3$ added $TiO(OH)_2$ | M1 |
| 9.2 ml $AgNO_3$ added $TiO(OH)_2$ | M2 |
| 13.8 ml $AgNO_3$ added $TiO(OH)_2$ | M3 |

## 4.2. CHARACTERIZATION

### 4.2.1. X-ray Diffraction (XRD)

The XRD patterns of the three different series of powders were taken. The changes in lattice parameters of the powders were calculated by using UnitCell software and XRD data. The software is a least squares refinement program which retrieves unit cell constants from experimental diffraction data.

Crystallite size was calculated by applying the Debye-Scherrer formula on characteristic peaks of $TiO_2$ powders. According to Debye-Scherrer formula (Maurya and Chauhan, 2011);

$$D=\frac{0.9\times\lambda}{\beta\times cos\theta}$$

D corresponds to the crystal size, while λ is the wavelength of the x-ray used, β is the full width at half maximum (FWHM) and θ is the scattering angle. For the determination of β, NIST 640 Silicon powder was used for instrumental broadening. The following formula was used for calculation of β, the FWHM of peak corrected for instrumental broadening, (Takahashi et al., 2005);

$$\beta = \sqrt{B^2 - b^2}$$

B corresponds to FWHM of $TiO_2$ peak and b is the FWHM of the Si internal standard peak for same crystal planes.

The mass fraction of anatase and rutile phases were calculated by the below formulae (Raj and Viswanathan, 2009);

Anatase (%) = $[\ 0.79I_A\ /\ (I_R+0.79I_A)\ ] \times 100$

Rutile (%) = $\{\ 1\ /\ [\ (I_R+0.79I_A)\ /\ I_R\ ]\ \}$ X 100

where $I_A$ and $I_R$ the peak intensities of (101) and (110) for anatase and rutile respectively.

The XRD patterns of “P” series of powders are shown in Figure 4.2.1. The patterns indicate the characteristic (101) diffraction peak of anatase $TiO_2$ at 2θ of ~25.3° (JCPDS #21-1272) and the characteristic (110) diffraction peak of rutile $TiO_2$ 2θ ~27.4° (JCPDS #21-1276). In addition to $TiO_2$ peaks, the characteristic (-111) diffraction peak of silver oxide (AgO) at 2θ of 32.3°(JCPDS #89-3081) is detected in the patterns of $AgNO_3$ added powders, which imply the presence of Ag as AgO in these powders. The presence of Ag in oxide form due to the reactant atmosphere is not an uncommon situation (Kubacka et al., 2008). Similar results have been also reported by Chou, 2005; Kato et al., 2005; Page et al., 2007; Priya et al., 2009; and Wang et al., 2011. The intensity of AgO peak increased slightly as the $AgNO_3$ addition during ball milling is increased. The enlarged pattern for this peak is given at the top right of Figure 4.2.1.  The second biggest (111) diffraction peak of AgO overlaps with (103) peak of anatase phase at 2θ of 37.2°. The XRD analyses suggest that anatase and rutile are present in all P series of powders before and after Ag addition. No phase change was recognized in the powders after Ag loading by ball milling. Mass fraction was calculated approximately 85% and 15% for anatase and rutile phases respectively for all powders indicating the absence of phase transformation during milling.

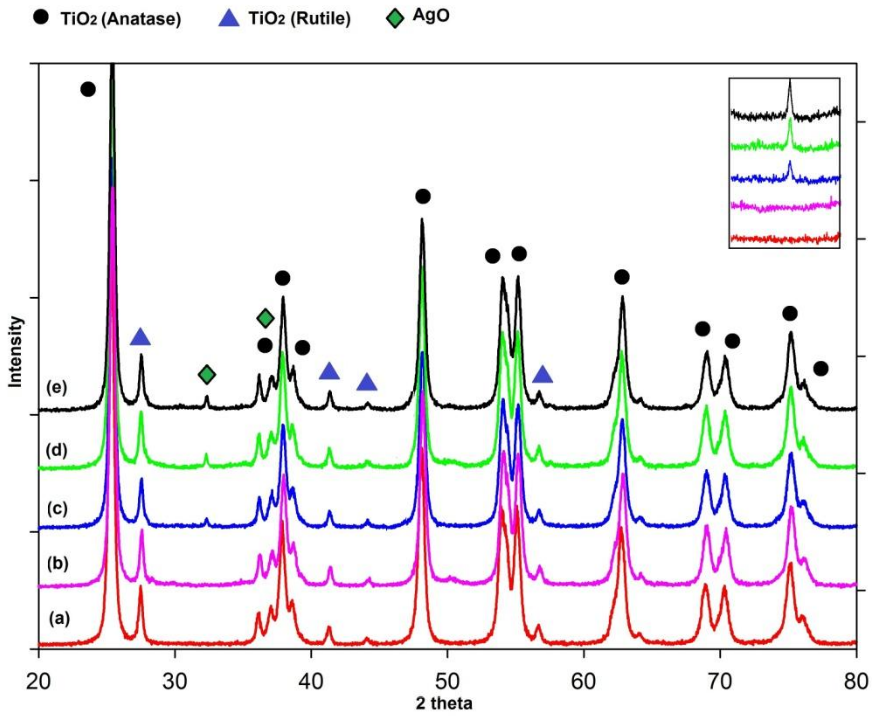

**Figure 4.2.1.** XRD patterns of the P series of powders **(a)** P, **(b)** P0, **(c)** P1, **(d)** P2, and **(e)** P3.

The changes in lattice parameters, lattice spacing and crystallite size for P, P0, P1, P2, and P3 are shown in Table 4.2.1.

**Table 4.2.1.** The lattice parameters, lattice spacing and crystallite size for the P series of powders for anatase and rutile phases.

| | | **P** | **P0** | **P1** | **P2** | **P3** | **JCPDS** |
|---|---|---|---|---|---|---|---|
| Anatase | **a (Å)** | 3.7852 | 3.7800 | 3.7834 | 3.7822 | 3.7831 | 3.7852 |
| | **c (Å)** | 9.5052 | 9.4884 | 9.4952 | 9.5098 | 9.4895 | 9.5139 |
| | **d (Å)** | 3.5047 | 3.4985 | 3.4955 | 3.4904 | 3.5006 | 3.5200 |
| | **Crystallite Size (nm)** | 23.30 | 23.62 | 23.22 | 23.92 | 23.16 | |
| Rutile | **a (Å)** | 4.5932 | 4.5854 | 4.593 | 4.5923 | 4.5905 | 4.5933 |
| | **c (Å)** | 2.9591 | 2.9544 | 2.9569 | 2.9570 | 2.9557 | 2.9592 |
| | **d (Å)** | 3.2380 | 3.2306 | 3.2296 | 3.2255 | 3.2343 | 3.2470 |
| | **Crystallite Size (nm)** | 27.84 | 28.10 | 27.71 | 28.78 | 28.25 | |

The calculated lattice parameter and lattice spacing values agree well with the values given in JCPDS cards of the anatase and rutile phases. After ball milling, “a” and “c” lattice parameter values for anatase and rutile phases remained almost the same. The minor changes can be attributed to mechanical milling since milling energy causes plastic deformation leading to lattice distortions (Shifu et al., 2008). After Ag addition lattice spacing and crystallite size were almost the same especially for anatase phase. This may lead to the conclusion that Ag did not get into the $TiO_2$ lattice. The expansion of $TiO_2$ cell due to the large ionic radius (1.24 Å; Tayade et al., 2006) of Ag (Liu, 2003; Wang et al., 1999) or the shrinkage due to the production of the deficiency of O vacancies in $TiO_2$ caused by the doping of metal ions with less oxidative states than IV of $TiO_2$ (Liu, 2003) were not observed for P series of powders.

Observation of no significant change in the 2θ values of the characteristic (101) diffraction peak of anatase $TiO_2$ and the characteristic (110) diffraction peak of rutile $TiO_2$ after Ag loading suggests that Ag did not doped into the $TiO_2$ lattice either in anatase or rutile phase.

The XRD patterns of the “N” series of powders are shown in Figure 4.2.2. The patterns indicate the characteristic (101) diffraction peak of anatase $TiO_2$ at 2θ of ~25.3° (JCPDS #21-1272). In addition to anatase $TiO_2$ peaks, a small but noticeable (-111) diffraction peak of AgO at 2θ of 32.3° (JCPDS #89-3081) is detected in the patterns of N2 and N3. The characteristic (110) diffraction peak of rutile $TiO_2$ at 2θ of ~27.4° (JCPDS #21-1276) is absent in all patterns. AgO is not identified in the pattern of N1 since amount of Ag present in this powder is very low and AgO peak having very low intensity for higher amounts of $AgNO_3$ addition is vanished in background. The intensity of AgO peak increased slightly as the $AgNO_3$ addition during ball milling is increased. The enlarged pattern for this peak is given at the top right of Figure 4.2.2. Again, the characteristic (111) diffraction peak of AgO is unseen in the XRD pattern since it overlaps with (103) peak of anatase phase at 2θ of 37.04°. The XRD analyses suggest that anatase $TiO_2$ is present; but, rutile $TiO_2$ does not exist in all N series of powders before and after Ag loading. No phase change was recognized in the powders after Ag loading by ball milling.

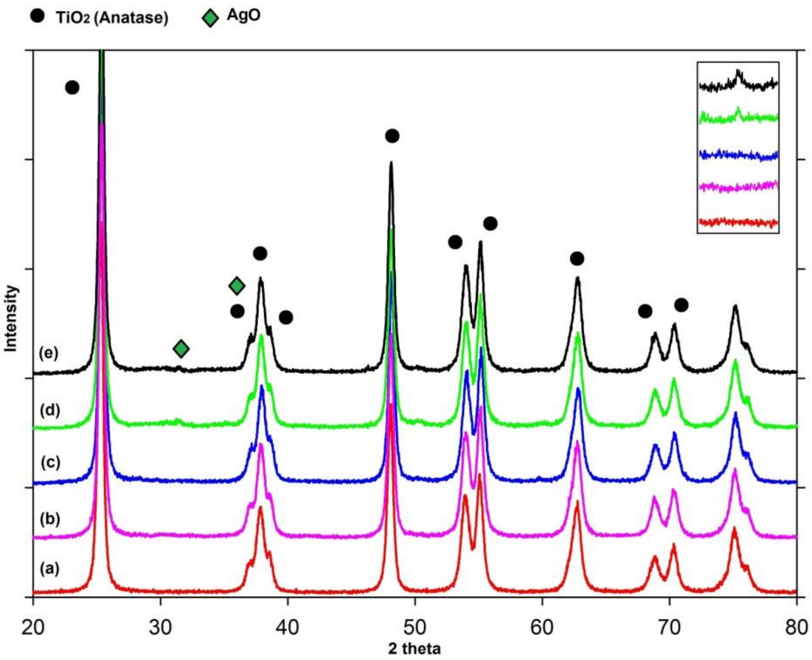

**Figure 4.2.2.** XRD patterns of the N series of powders **(a)** N, **(b)** N0, **(c)** N1, **(d)** N2, and **(e)** N3.

The changes in lattice parameters, lattice spacing and crystallite size for N, N0, N1, N2, and N3 are shown in Table 4.2.2.

**Table 4.2.2** The lattice parameters, lattice spacing and crystallite size for the N series of powders.

| | N | N0 | N1 | N2 | N3 |
|---|---|---|---|---|---|
| **a(Å)** | 3.7850 | 3.7818 | 3.7835 | 3.7822 | 3.7832 |
| **c(Å)** | 9.5098 | 9.5189 | 9.4953 | 9.5098 | 9.4896 |
| **d (Å)** | 3.5018 | 3.4966 | 3.5002 | 3.5035 | 3.5017 |
| **Crystallite Size (nm)** | 22.63 | 22.17 | 22.22 | 22.11 | 22.13 |

The calculated lattice parameter and lattice spacing values of the N series of powders data agree well with the JCPDS card of the anatase phase. “a” lattice parameters remained almost same before and after milling as well as after Ag loading. A slight elongation on “c” axis was observed after ball milling due to milling energy. For all ball milled powder with or without Ag addition, crystallite size is almost the same and slightly smaller than the starting powder which may be due to the production of deficiency of O vacancies in $TiO_2$ caused by the addition of metal ions with less oxidative states than IV of $TiO_2$ (Liu, 2003). This finding may lead to the conclusion that Ag did not doped into the $TiO_2$ lattice. No shift in the characteristic (101) diffraction peak of anatase $TiO_2$ after Ag loading implies that Ag did not doped into the $TiO_2$ lattice.

The XRD patterns of the “M” series of powders are shown in Figure 4.2.3. The patterns indicate the characteristic (101) diffraction peak of anatase $TiO_2$ at 2θ of ~25.3° (JCPDS #21-1272). In addition to anatase $TiO_2$ peaks, a small but noticeable (-111) diffraction peak of AgO at 2θ of 32.3° (JCPDS #89-3081) is detected in the patterns of M2 and M3. The characteristic (110) diffraction peak of rutile $TiO_2$ at 2θ of ~27.4° (JCPDS #21-1276) is absent in all patterns. AgO is not identified in the pattern of M1 since amount of Ag present is very low and AgO peak that also has very low intensity for higher amounts of $AgNO_3$ addition is vanished in background. The intensity of AgO peak increased slightly as the $AgNO_3$ addition during ball milling is increased. The enlarged pattern for this peak is given at the top right of Figure 4.2.3. The characteristic (111) diffraction peak of Ago could not be seen in the XRD pattern since it overlaps with (103) peak of anatase phase at 2θ of 37.04°. The XRD analyses suggest that anatase $TiO_2$ is present but rutile $TiO_2$ does not exist in all M series of powders before and after Ag loading. No phase change was recognized in the powders after Ag loading by ball milling.

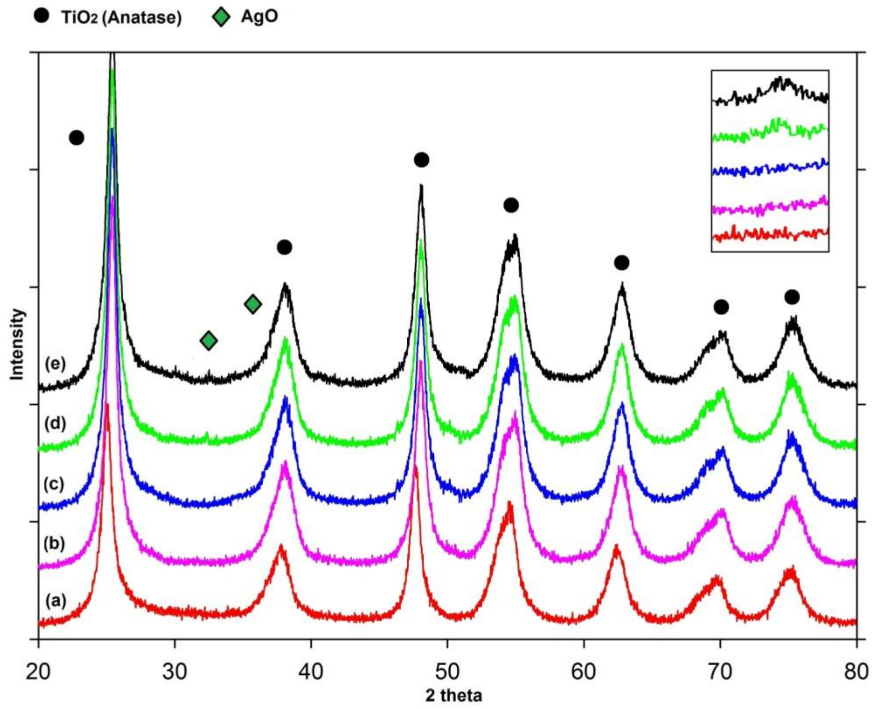

**Figure 4.2.3.** XRD patterns of the M series of powders **(a)** M, **(b)** M0, **(c)** M1, **(d)** M2, and **(e)** M3

The changes in lattice parameters, lattice spacing and crystallite size for M, M0, M1, M2, and M3 are shown in Table 4.2.3.

**Table 4.2.3** The lattice parameters, lattice spacing and crystallite size for the M series of powders.

| | M | M0 | M1 | M2 | M3 |
|---|---|---|---|---|---|
| **a(Å)** | 3.7877 | 3.7801 | 3.7845 | 3.7845 | 3.7855 |
| **c(Å)** | 9.4879 | 9.5079 | 9.4956 | 9.5080 | 9.5303 |
| **d (Å)** | 3.5006 | 3.5027 | 3.5004 | 3.4963 | 3.5005 |
| **Crystallite Size (nm)** | 9.89 | 9.84 | 9.73 | 10.23 | 9.90 |

The calculated lattice parameter and lattice spacing values of the M series of powders agree well with the values given in the JCPDS card of the anatase phase. With ball milling, “a” lattice parameters remained almost the same but some amount of deviation was observed in the “c” parameters indicating a lattice distortion on c axis due to ball milling. After Ag loading, cell volume, “a” and “c” lattice parameters increased, which may be attributed to the large ionic radius of Ag leading to the expansion of $TiO_2$ cell (Liu, 2003; Wang et al., 1999). For M2 powder, lattice spacing was decreased while crystallite size increased considerably suggesting that some amount of Ag may be incorporated into the $TiO_2$ lattice.

No contamination from the milling media was noticed in the XRD analysis of powders signifying that the mechanical milling process did not bring any phase transformation or impurity effect.

### 4.2.2. Scanning Electron Microscope (SEM) and Energy Dispersive Spectroscopy (EDS)

The surface morphologies of “P” series of powders are shown in the SEM images shown in Figure 4.2.4

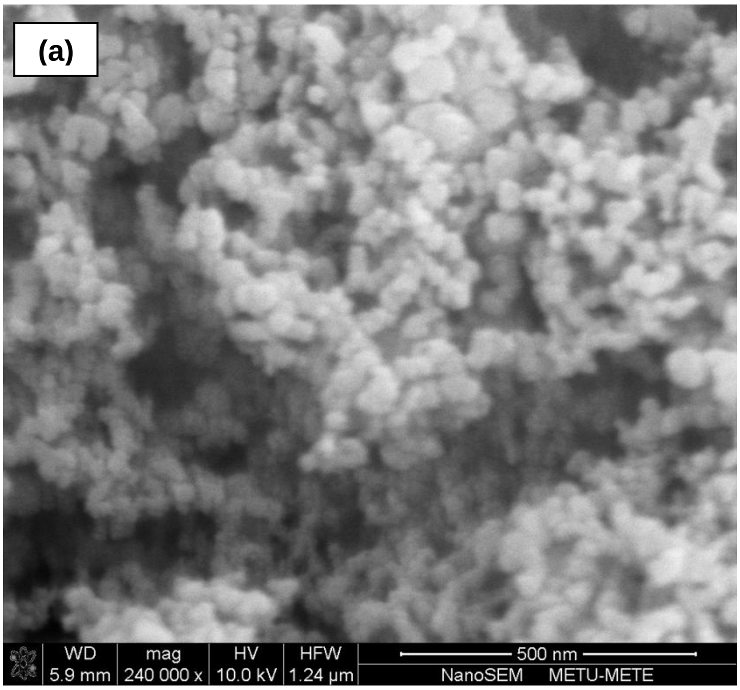
(a)
WD 5.9 mm
mag 240 000 x
HV 10.0 kV
HFW 1.24 µm
500 nm
NanoSEM METU-METE

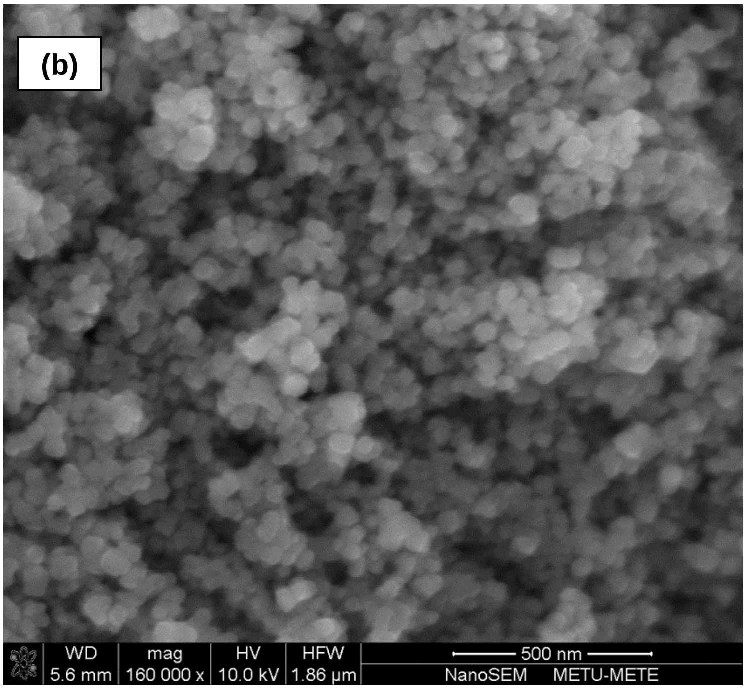
(b)
WD 5.6 mm
mag 160 000 x
HV 10.0 kV
HFW 1.86 µm
500 nm
NanoSEM METU-METE

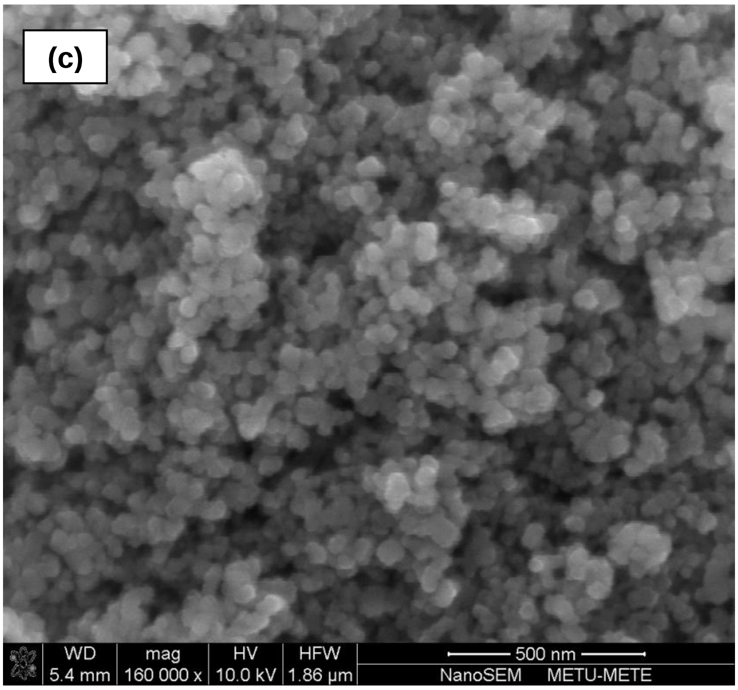
(c)
WD
5.4 mm
mag
160 000 x
HV
10.0 kV
HFW
1.86 µm
500 nm
NanoSEM
METU-METE

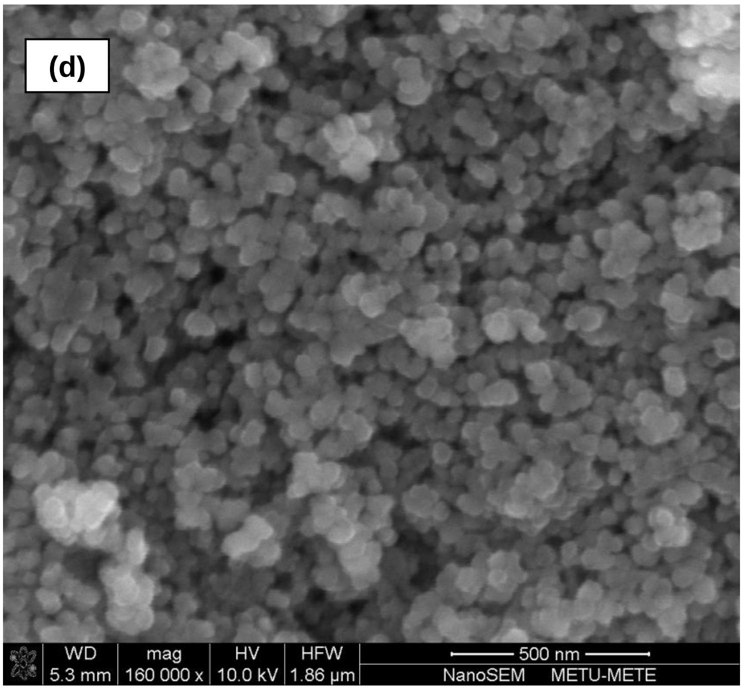
(d)
WD
5.3 mm
mag
160 000 x
HV
10.0 kV
HFW
1.86 µm
500 nm
NanoSEM
METU-METE

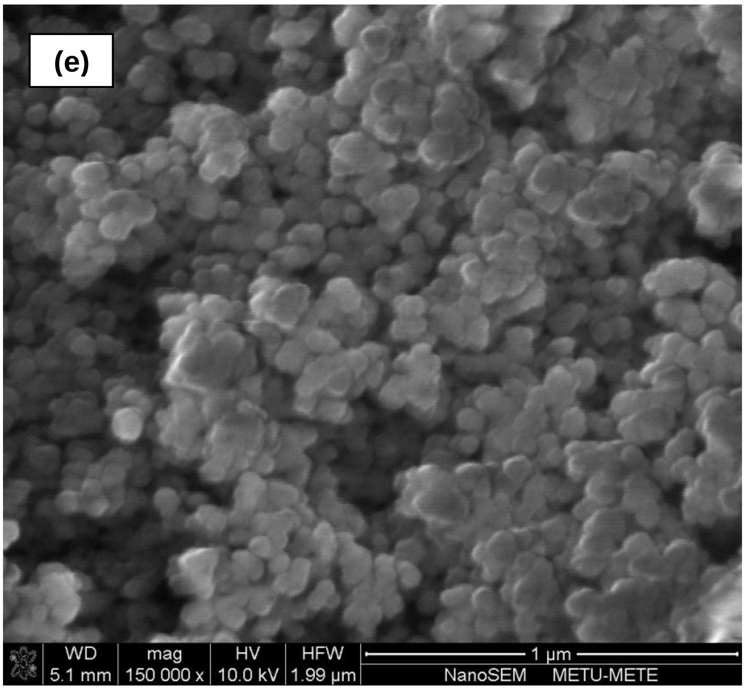

**Figure 4.2.4.** SEM images of the P series of powders **(a)** P (240000x), **(b)** P0 (160000x), **(c)** P1 (160000x), **(d)** P2 (160000x), and **(e)** P3 (150000x).

SEM analysis revealed that the particles in all P series of powders are nearly spherical in shape, uniform in size and agglomerated. The surface morphology and shapes of particles did not change after ball milling.

Particle size of the powders as determined from SEM images by taking the size average of different particles taken from different places in the image are shown in Table 4.2.3. These results do not represent the average particle size of the powders. They are the sizes of single particles that were not agglomerated and could be detected clearly from SEM images.

**Table 4.2.3**. Particle size of the P series of powders as determined from SEM images.

| Powder | P | P0 | P1 | P2 | P3 |
|---|---|---|---|---|---|
| Particle Size (nm) | 56.6 | 43.4 | 49.6 | 51.7 | 54.7 |

P-25 powder generally consists of particles around 50 nm in diameter. However, as shown in Table 3.1.1., the manufacturer of this powder quoted particle size as 21 nm. Therefore particle size data obtained from the SEM images may not be true, but they have been measured for comparison of the sizes of particles before and after ball milling and Ag loading. As expected, particle size of P-25 powder decreased after ball milling without Ag loading since ball milling process causes particle size refinement. However, particle size of the powders increased for a few nanometers as the $AgNO_3$ solution was added to P-25 powder during ball milling. This is attributed to the mechanical energy in milling. The mechanical energy accelerated the aggregation since the fresh surfaces exposed by the milling lowers their high surface energy by agglomeration (Rattanakam and Supothina, 2009; Yin et al., 2006; Z. Zhou et al., 2005). Moreover, the increase in particle size may be due to the coating of AgO onto surface of $TiO_2$ particles (Keleher et al., 2002).

Data obtained from EDS analysis of the “P” series of powders are given in Table 4.2.4. As expected, amount of Ag in the powders increases as the amount of $AgNO_3$ solution added during ball milling is increased.

**Table 4.2.4.** Results of EDS analysis of P series of powders.

|  | P | P0 | P1 | P2 | P3 |
|---|---|---|---|---|---|
| Element | Wt% | Wt% | Wt% | Wt% | Wt% |
| O K | 54.84 | 44.48 | 45.29 | 42.40 | 36.83 |
| AgL | 0 | 0 | 0.41 | 1.28 | 1.88 |
| TiK | 45.16 | 55.52 | 54.30 | 56.32 | 61.35 |

The surface morphologies of “N” series of powders are shown in the SEM images shown in Figure 4.2.4

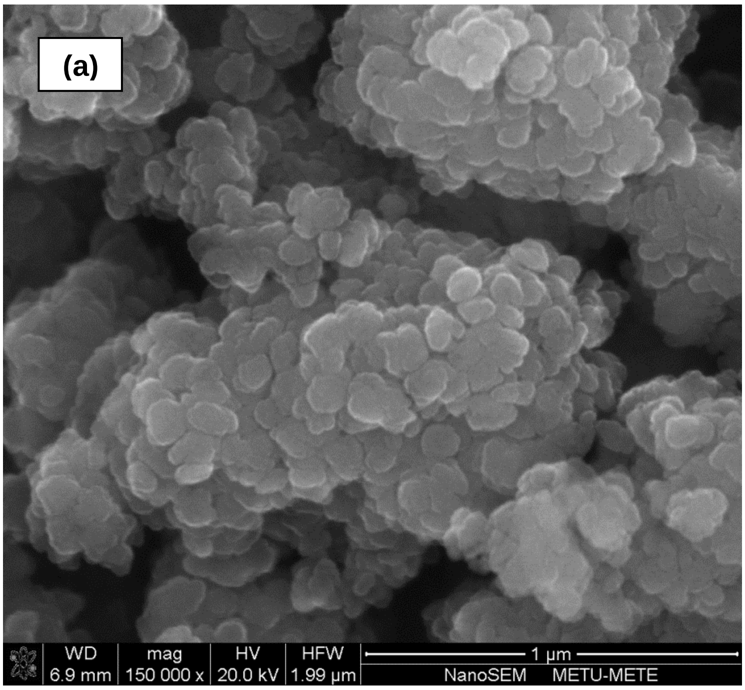

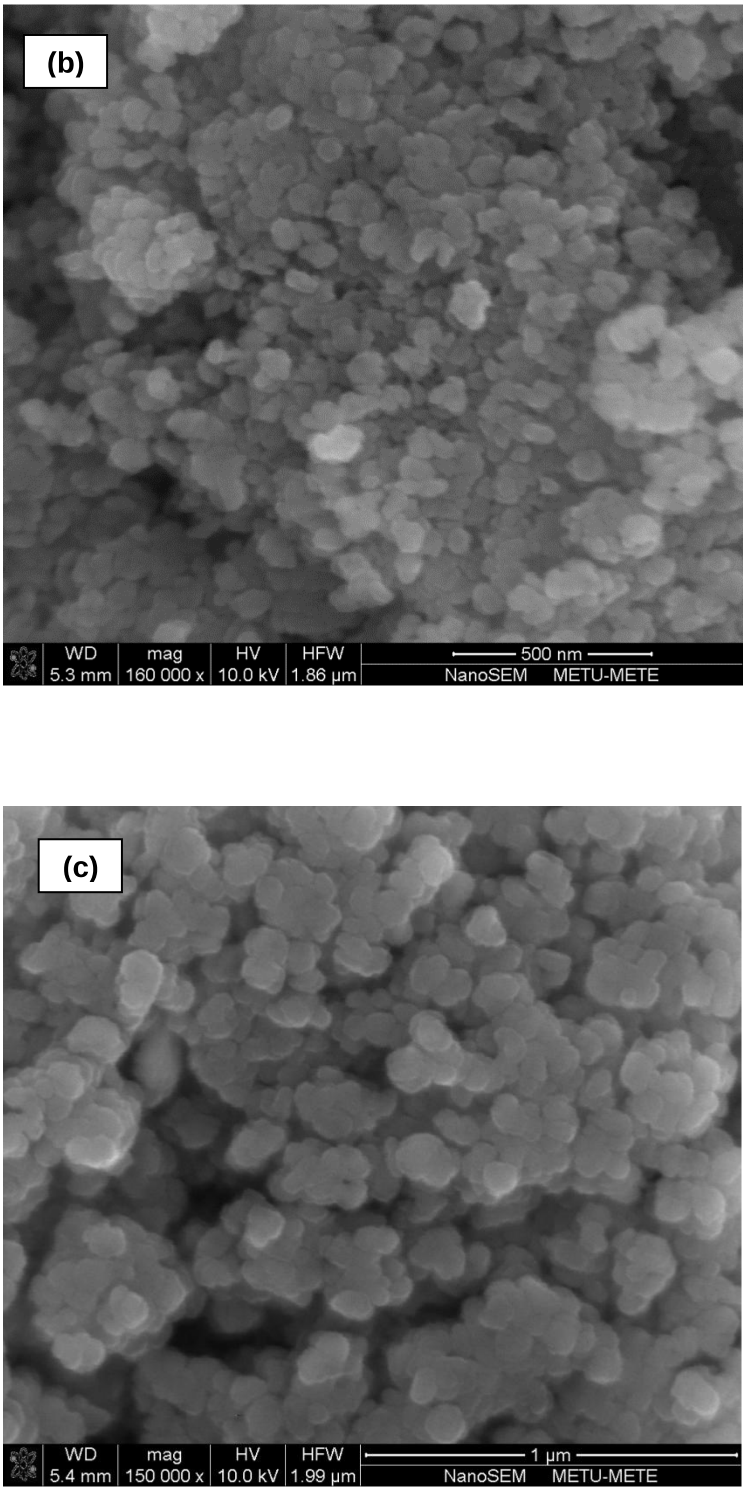
(b)
WD 5.3 mm
mag 160 000 x
HV 10.0 kV
HFW 1.86 µm
500 nm
NanoSEM METU-METE
(c)
WD 5.4 mm
mag 150 000 x
HV 10.0 kV
HFW 1.99 µm
1 µm
NanoSEM METU-METE

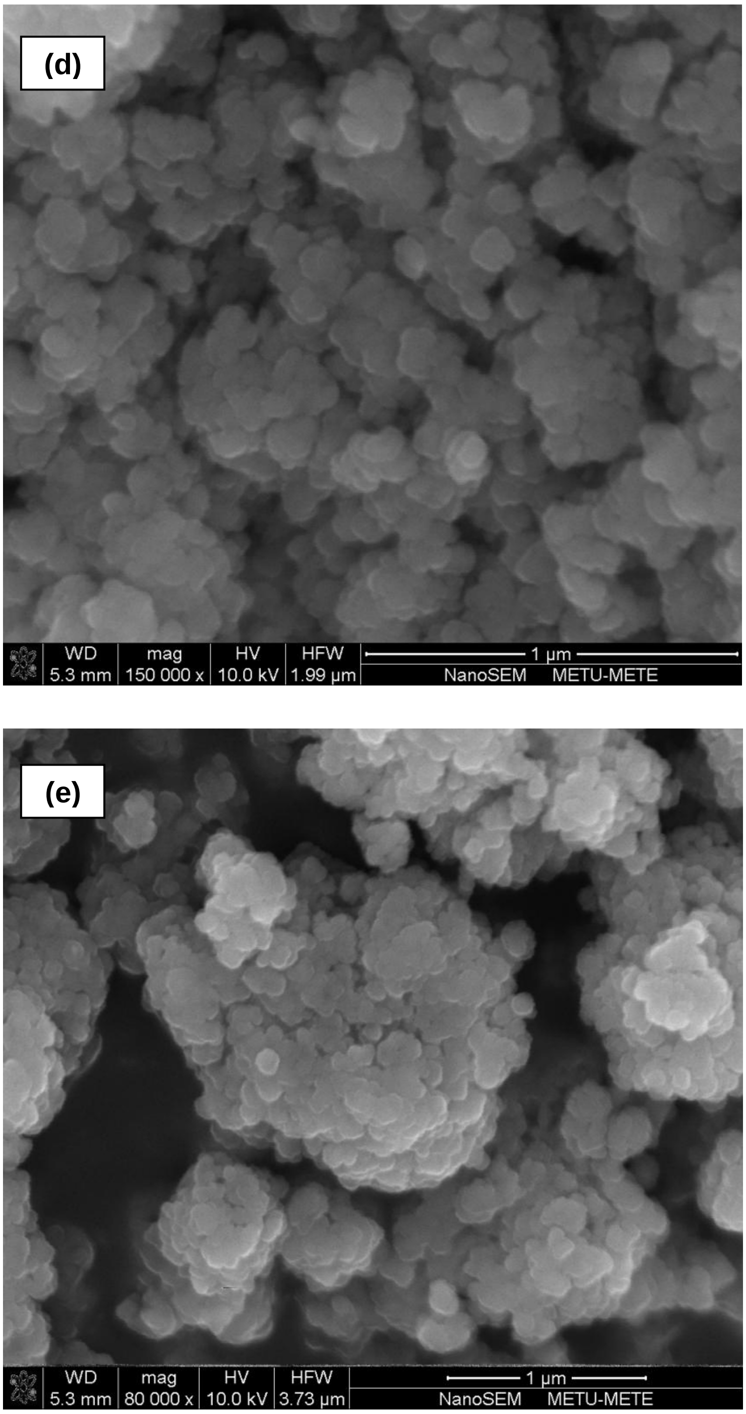

**Figure 4.2.5.** SEM images of the N series of powders **(a)** N (150000x), **(b)** N0 (160000x), **(c)** N1 (150000x), **(d)** N2 (150000x) and **(e)** N3 (80000x).

SEM analysis revealed that the particles in all N series of powders are nearly spherical in shape and rather agglomerated. The particles in the powders milled without $AgNO_3$ seem less agglomerated than the ones in the starting powders. The surface morphology and shapes of particles did not change after ball milling.

Particle size of the powders as determined from SEM images by taking the size average of different particles taken from different places in the image are shown in Table 4.2.5.

**Table 4.2.5.** Particle size of the N series powders as determined from SEM images.

| Powder | N | N0 | N1 | N2 | N3 |
|---|---|---|---|---|---|
| Particle Size (nm) | 108.8 | 91.6 | 94.5 | 101.8 | 107.9 |

NT-22 powder series generally consist of particles of 100 nm. Particle size of the powders increased for a few nanometers as the $AgNO_3$ addition during ball milling is increased. Again, the increase in particle size can be related to agglomeration induced by ball milling or AgO coating as mentioned for P series of powders.

When a comparison is made between the P and N series of powders, it is obvious that the N series of powders are coarser than the P series of powders. The difference in particle size of these series of powders is related to the size of the starting powders. As presented in Table 3.1.1, P-25 powder was finer than N-22 powder. The SEM images and particle size calculations confirm this information as well.

Data obtained from EDS analysis of the “N” series of powders are given in Table 4.2.6. As expected, amount of Ag in the powders increases as the amount of $AgNO_3$ solution added during ball milling is increased.

**Table 4.2.6.** Results of EDS analysis of N series of powders.

| | N | N0 | N1 | N2 | N3 |
|---|---|---|---|---|---|
| Element | Wt% | Wt% | Wt% | Wt% | Wt% |
| O K | 48.36 | 51.19 | 47.78 | 49.70 | 56.56 |
| AgL | 0 | 0 | 0.49 | 0.69 | 0.91 |
| TiK | 51.64 | 48.81 | 51.73 | 49.61 | 42.53 |

The surface morphologies of “M” series of powders are shown in the SEM images in Figure 4.2.4.

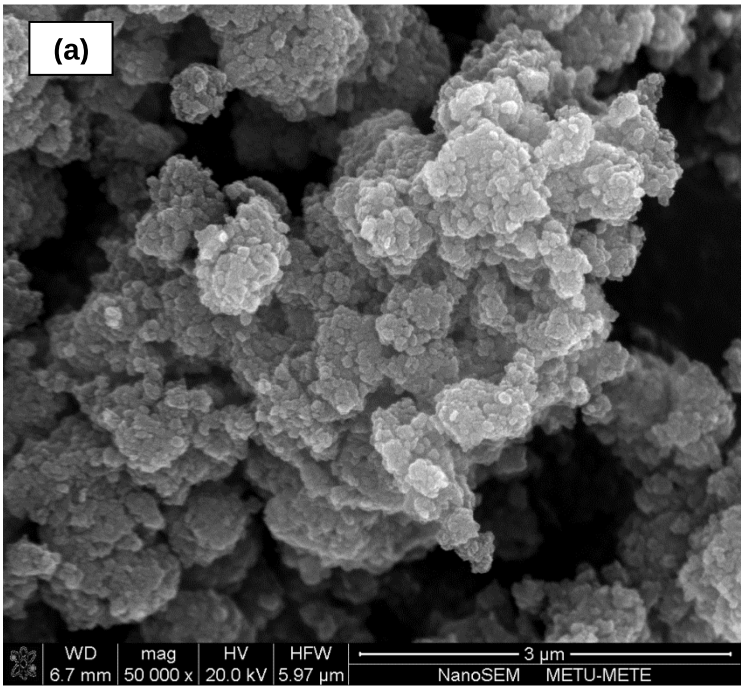

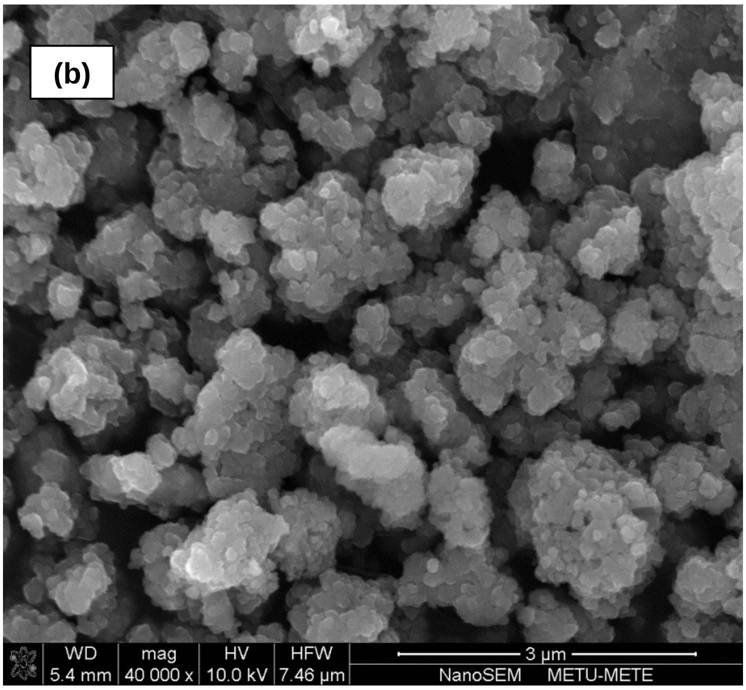
(b)
WD
5.4 mm
mag
40 000 x
HV
10.0 kV
HFW
7.46 µm
3 µm
NanoSEM
METU-METE

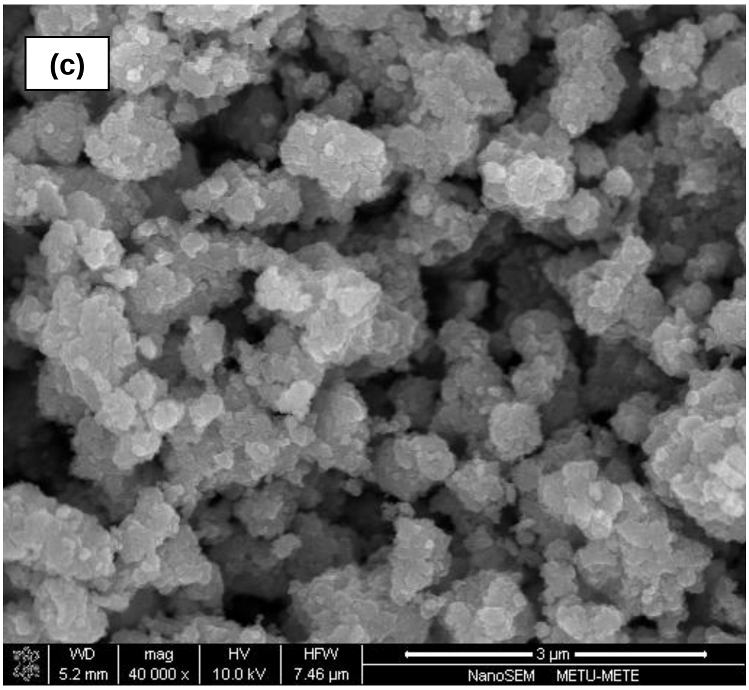
(c)
WD
5.2 mm
mag
40 000 x
HV
10.0 kV
HFW
7.46 µm
3 µm
NanoSEM
METU-METE

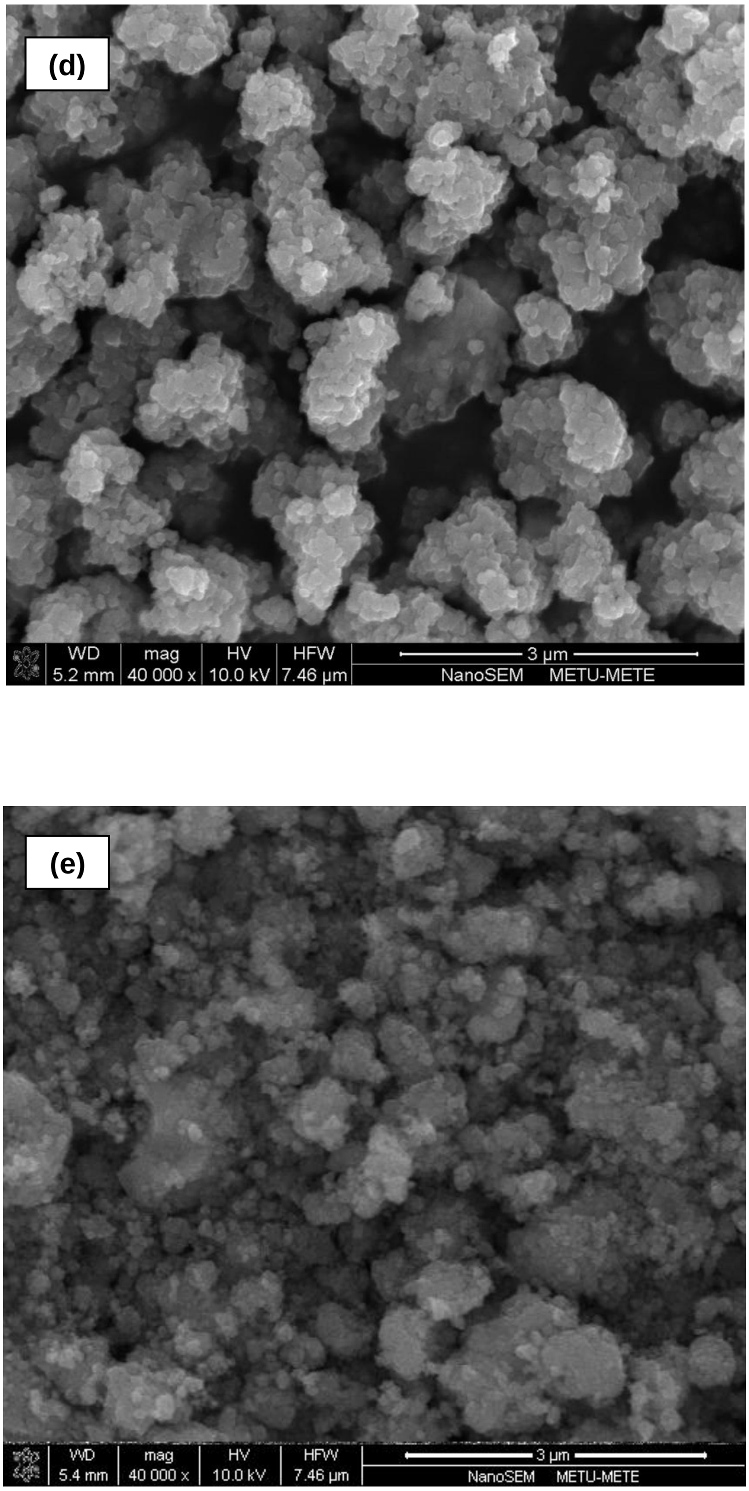

**Figure 4.2.6.** SEM images of the M series of powders **(a)** M (50000x), **(b)** M0 (40000x), **(c)** M1 (50000x), **(d)** M2 (40000x) and **(e)** M3 (40000x).

SEM analysis revealed that the particles in all M series of powders are nearly spherical in shape and agglomerated. The surface morphology and shapes of particles did not change with ball milling.

Average particle size of the powders as determined from SEM images by taking the size average of different particles taken from different places in the image are shown in Table 4.2.7.

**Table 4.2.7.** Particle size of the M series of powders as determined from SEM images.

| Powder | M | M0 | M1 | M2 | M3 |
|---|---|---|---|---|---|
| Particle Size (nm) | 94.3 | 73.9 | 93.1 | 96.4 | 99.7 |

It is observed that, just like for P-25 and NT-22, as the amount of Ag loading increases the particle size also increases for a few nanometers due to agglomeration and coating of AgO onto the surface of $TiO_2$ particles. Similar to P and N series, the particle size decreased with ball milling however Ag addition deteriorated the particle size reduction.

Data obtained from EDS analysis of the M series of powders are given in Table 4.2.8. Amount of Ag present increases as the $AgNO_3$ during ball milling increases.

**Table 4.2.8.** Results of EDS analysis of M series of powders.

| | M | M0 | M1 | M2 | M3 |
|---|---|---|---|---|---|
| Element | Wt% | Wt% | Wt% | Wt% | Wt% |
| O K | 53.90 | 58.60 | 53.34 | 52.56 | 52.07 |
| AgL | 0 | 0 | 0.64 | 1.05 | 1.73 |
| TiK | 46.10 | 41.40 | 46.02 | 46.39 | 46.20 |

SEM examinations revealed that the P series of powders were smaller than the N and M series of powders. The P series of powders needed more harsh and intensive grinding by agate with pestle after drying. After drying, new mechanical and chemical bonds are formed between particles and it is difficult to break these bonds and obtain the powders with the same structural properties. A comparison of the particle size observed from SEM for all the powders investigated in this study is given separately in Figure 4.2.7.

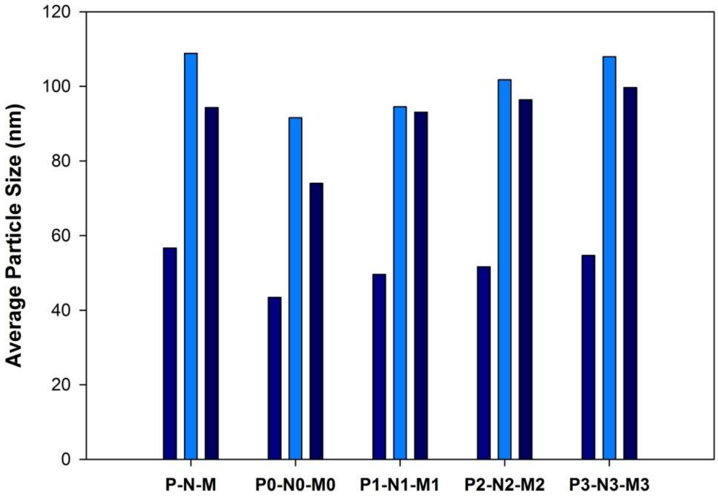

**Figure 4.2.7.** Particle size as determined from SEM images for the powders investigated in this study.

### 4.2.3. Particle Size

Average particle size measurement was employed for the starting powders, ball milled powders and Ag loaded powders exhibiting the best photocatalytic activity.

Particle size distributions for the powders P, P0 and P3 are shown in Figure 4.2.8.

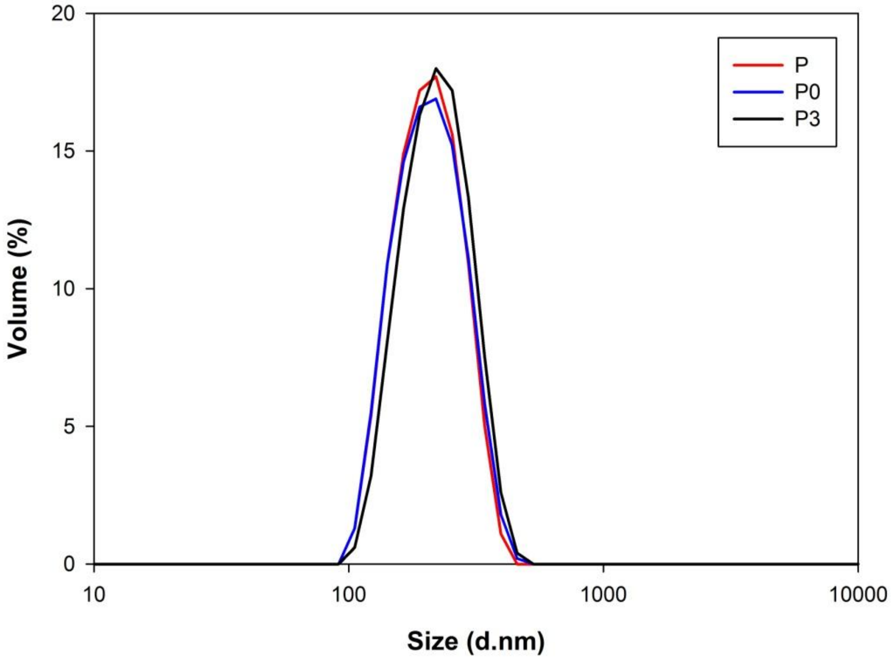

**Figure 4.2.8.** Particle size distribution for the powders P, P0 and P3.

Ball milling did not cause a considerable change on particle size distribution of P series of powders. Average particle size of starting powder P-25 was measured as 216.2 nm. Ball milled P-25 without Ag loading had an average particle size of 204.6 nm and Ag loaded particles had an average of 212.6 nm. The values of particle size measured by particle size analyser do not coincide with the ones determined from SEM images. The disagreement in the particle size data between these measurement techniques are basically due to the agglomeration of particles so that the data taken from particle size analyser are consistently bigger that that taken from SEM images. Although solutions taken from ball mill were tried to be dispersed using an ultrasonic convertor before the analysis, complete dispersion of the particles was not accomplished. Individual particles with 50 nm in length were observed in SEM images. However, the smallest particles detected by particle size analyser have particles size around 90 nm. It is assumed that amount of small particles that can be observed through SEM examination are very low and were not detected by wet particle size analysis method. According to technical data P-25 supposed to have an average particle size of 21 nm. However it is noted that particle size measurements done in colloidal systems do not correspond to that value due to differences in measurement techniques (Fernández-ibáñez et al., 1999). It can be noted that the P series of powders consist of particles around 50 nm and the average particle size for this series is 210 nm.

Particle size distributions for the powders N, N0 and N3 are shown in Figure 4.2.9.

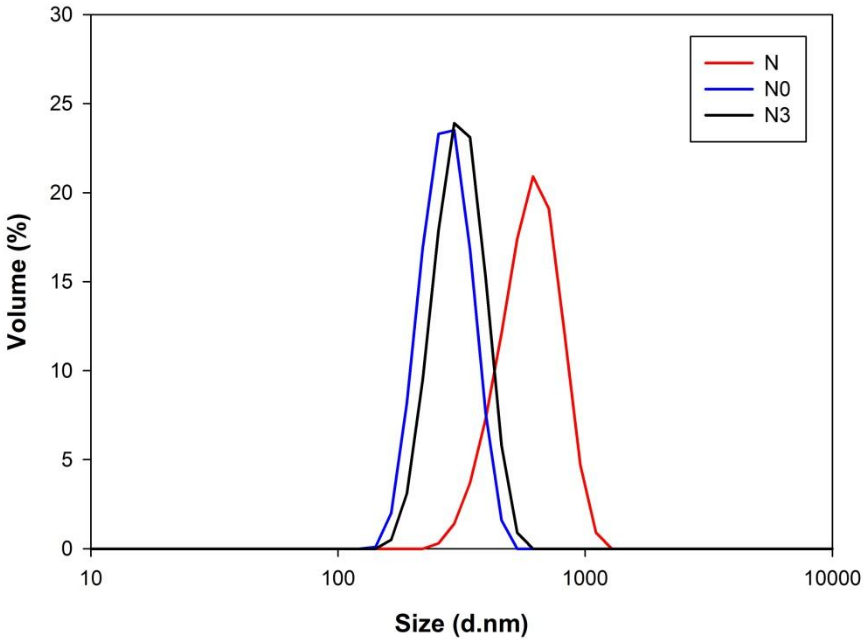

**Figure 4.2.9.** Particle size distributions for the powders N, N0 and N3.

For the N series of powders ball milling was effective for particle size reduction. Starting powder NT-22 has an average particle size of 555 nm, while after ball milling particle size reduced to 364.1 nm. Ball milling with Ag loading resulted an average of 407.9 nm of particle size. Individual particles with 100 nm in length were observed in SEM images. However, the smallest particles detected by particle size analyser have particle size around 140 nm. It can be noted that the N series of powders consist of particles around 100 nm and the average particle size is 400 nm.

Particle size distributions for the powders M, M0, and M3 are shown in Figure 4.2.10.

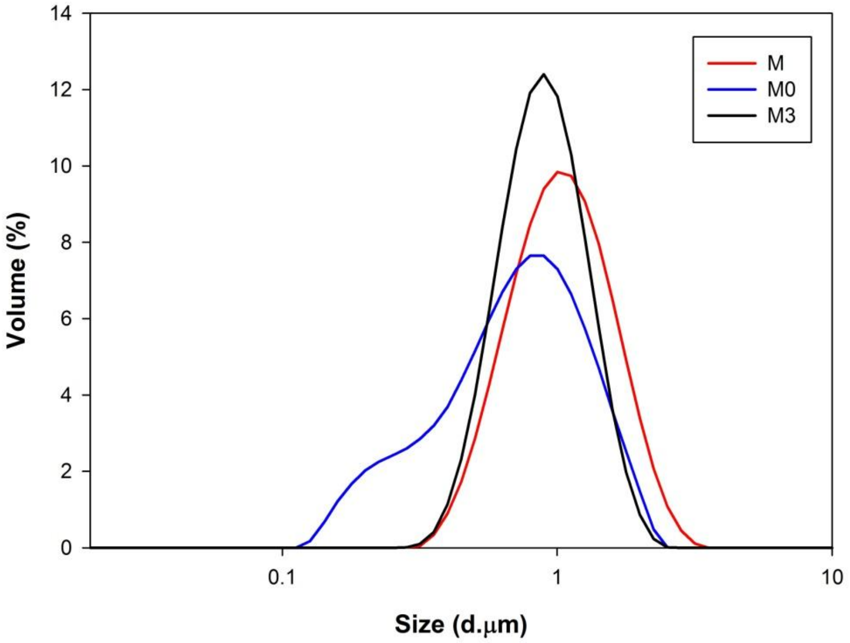

**Figure 4.2.10.** Particle size distributions for the powders M, M0, and M3.

For the M series of powders ball milling was effective for particle size reduction especially without Ag addition. Starting powder metatitanate has an average particle size of 1.115 μm, while after ball milling average particle size reduced to 0.769 μm. Ball milling with Ag loading resulted an average of 0.937 μm of particle size. Particles with sizes around 90 nm were observed in SEM analysis but, minimum particles that could be detected through particle size analyser were about 140 nm. It can be noted that, the M series of powders consist of particles around 100 nm and the average particle size is 1 μm.

Although there is a disagreement in the particle size data between these two measurement techniques, the trend of particle size refinement between all series of powders was the same. That is, ball milled powders had smaller size than starting powders but larger size than Ag loaded powders. This finding is related to the formation of AgO on $TiO_2$ powders. As the particle size decrease, new surfaces with high energy form and agglomeration occurs in order to lower the energy (Yin et al., 2007). As a newly formed surface AgO also wants to lower the energy and may help to accelerate the agglomeration of $TiO_2$ powders.

According to the average particle size data, P-25 can be classified as fine, NT-22 as medium and metatitanate as coarse. Since the P series of powders are finer in particle size then the N and M series of powders according to particle size analysis and SEM data, they are expected to have superior photocatalytic properties due to the fact that particle size is one of the most important factors on photocatalytic performance as mentioned in Section 2.3.1.

### 4.2.4. Brunauer-Emmett-Teller (BET) Surface Area

Results for BET specific surface area measurements of the P series of powders are shown in Table 4.2.9.

**Table 4.2.9**. BET Specific Surface Area for the P series powders.

| Powder | BET Specific Surface Area ($m^2/g$) |
|---|---|
| P | 61.62 |
| P0 | 61.11 |
| P1 | 54.29 |
| P2 | 46.96 |
| P3 | 42.97 |

Specific surface area of starting powder P-25 was measured as 61.62 $m^2/g$. This measurement is in agreement with the values given in technical datasheet as 55 ± 15 $m^2/g$. The specific surface area after ball milling was more or less the same. It should be noted that size for individual particles decreases via ball milling, however due to the surface energy induced by ball milling agglomeration of particles takes place in order to lower surface energy (Woo et al., 2007). Specific surface area also decreased after Ag loading. The decrease in surface area after Ag loading was also noted by Iliev et al., 2006 and Kondo and Jardim, 1991. The decrease in specific surface area after Ag loading may be related to the increase in particle size due to Ag coating (Keleher et al., 2002) or due to blocking of fine capillaries of parent $TiO_2$ surface by metal film islands (Sakthivel et al., 2004; Sobana et al., 2006).

Results for BET specific surface area measurements of the N series of powders are shown in Table 4.2.10.

**Table 4.2.10.** BET Specific Surface Area for the N series of powders.

| Powder | BET Specific Surface Area ($m^2/g$) |
|---|---|
| N | 78.53 |
| N0 | 81.64 |
| N1 | 71.38 |
| N2 | 71.22 |
| N3 | 64.89 |

Specific surface area of starting powder NT-22 was measured as 78.53 $m^2/g$. This measurement is in agreement with the values given in technical datasheet as 60 - 80 $m^2/g$. The specific surface area for powder N0 was a little larger than the starting powder which indicates that particle refinement was efficient as a result of ball milling. After Ag loading, specific surface area decreased. The lowest specific surface area was obtained for powder N3 as 64.89 $m^2/g$. The decrease in specific surface area after Ag addition was also reported before by Kondo and Jardim, 1991, Keleher et al., 2002, Sakthivel et al., 2004 and Sobana et al., 2006.

Results for BET specific surface area measurements of the M series of powders are shown in Table 4.2.11.

**Table 4.2.11**. BET Specific Surface Area for the M series of powders.

| Powder | BET Specific Surface Area ($m^2/g$) |
|---|---|
| M | 221.0 |
| M0 | 343.8 |
| M1 | 254.8 |
| M2 | 289.7 |
| M3 | 271.0 |

Specific surface area of starting powder $TiO(OH)_2$ was measured as 221.0 $m^2/g$. This powder did not have the specific surface area value on its technical data sheet. Specific surface area of this powder is reported around 200 $m^2/g$ by Kim et al., 2004, and Kim et al., 2008. The specific surface area increased for M0 which indicates this powder was ground to smaller sizes during ball milling. After Ag loading, specific surface area decreased. The lowest specific surface area was obtained for powder M3 as 271.0 $m^2/g$.

For all series of powders, there is a direct relation between particle size and surface area. Effect of ball milling and Ag loading to $TiO_2$ powders were observed and results are consistent with particle size analysis measurements.

## 4.3. PHOTOCATALYTIC ACTIVITY

Photocatalytic activity of all the investigated powders was measured according to the procedure given in Section 3.3.1. Results for different series of powders are presented in the subsections below.

### 4.3.1.Photocatalytic Activity of the P series of Powders in MO Solution

The absorbance spectra obtained after 60 min of UV illumination for the P series of powders are given in Figure 4.3.1. The absorbance spectra obtained after 60 min of UV illumination for the MO solution was included in the figure for comparison purposes.

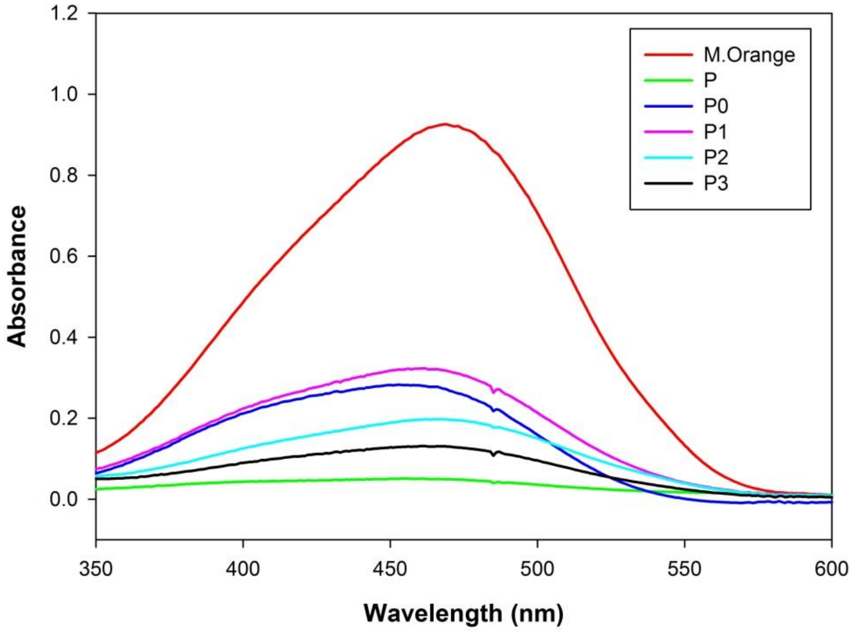

**Figure 4.3.1.** Absorbance spectra for the P series of powders.

In the P series of powders, the starting P-25 powder gave the best results in terms of the degradation of MO. Without UV irradiation, P series of powders did not provide any remarkable degradation, which indicates that all the further degradation upon UV will be caused by photocatalytic reaction only. Ag loading to this powder deteriorated the degradation of MO implying that photocatalytic efficiency of starting P-25 powder decreased when some amount of Ag was loaded to it. Starting P-25 powders decomposed 94.49% of MO in the MO solution in 60 min. MO degradation by P-25 was reported differently by different researchers. For instance, in one study (Tong et al., 2008) MO degradation was calculated as 70% in 1 hour UV irradiation, in another study (Guettaï and Amar, 2005) 50% of MO was degraded in 1 hour. The different values for degradation are related to the experimental details such as initial MO concentration, photocatalyst concentration or the power of UV lamp. However, the 94.49% decomposition by P-25 is not an unexpected result since P-25 is the most commonly used commercially available photocatalytic powder in the market. P-25 is a mixture of anatase and rutile phases. Although rutile is known to be less photocatalytic and expected to lower the activity, P-25 is one of the best known photocatalytic powders. According to previous studies, anatase and rutile particles exist separately in P-25 and it was proved that there is a synergistic effect between these two contacting phases. It was noted that the positive interaction of these two phases enhances the electron hole separation and so the total photoefficiency (Sun and Smirniotis, 2003). Ball milling may have a negative effect on the anatase-rutile interaction of P-25 powders since it was observed that milling did not enhance the photocatalytic efficiency of P-25 although particle size was slightly reduced.

Values for the degradation of MO in the MO solution for the P series of powders are given in Table 4.3.1. Among the Ag loaded P series of powders, P3 showed better photocatalytic efficiency than P1 and P2 as shown in Figure 4.3.2. 2. Results suggest that photocatalytic activity of the powder increases as the Ag loading is increased since Ag acts as electron traps and enhances the electron hole separation. Moreover, it also enhances the transfer of trapped electrons to the adsorbed $O_2$ acting as an electron acceptor (Sung-suh et al., 2004). This finding is an indication of and can be taken as the positive effect of Ag loading on photocatalytic properties.

**Table 4.3.1.** % MO Degradation of the P series of powders.

| | **%MO Degradation after** | | |
|---|---|---|---|
| **Powder** | 30 min (No UV) | 30 min (UV) | 60 min (UV) |
| P | 1.42 | 64.45 | 94.49 |
| P0 | 0.72 | 38.51 | 67.11 |
| P1 | 1.05 | 40.55 | 65.12 |
| P2 | 0.78 | 60.04 | 78.67 |
| P3 | 0.89 | 69.19 | 85.85 |

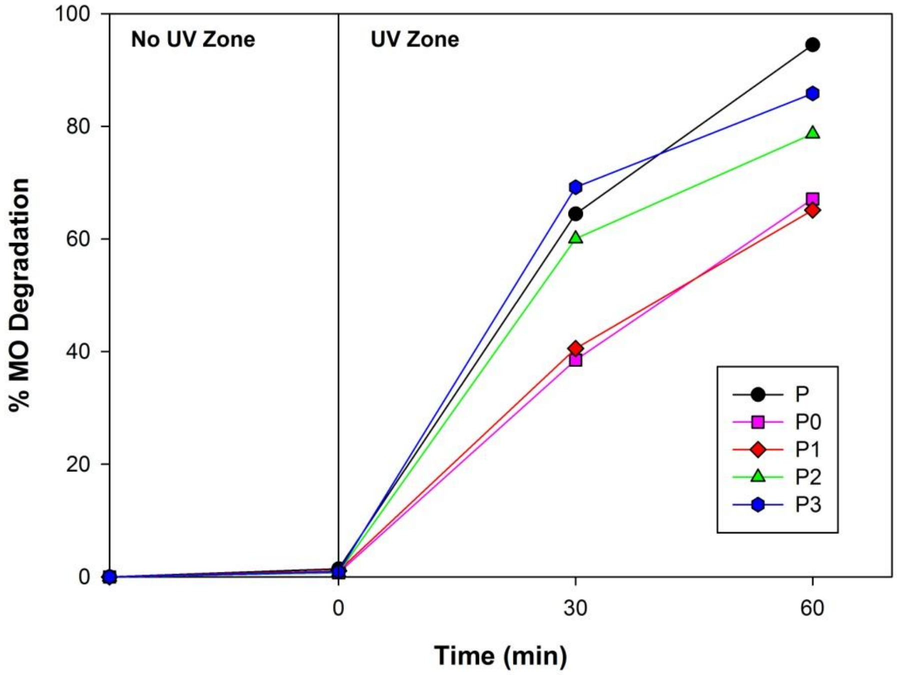

**Figure 4.3.2.** % MO Degradation for the P series of powders.

### 4.3.2.Photocatalytic Activity of the N series of Powders in MO Solution

The absorbance spectra obtained after 60 minutes of UV illumination for N series of powders are given in Figure 4.3.3. The absorbance spectra obtained after 60 min of UV illumination for the MO solution was included in the figure for comparison purposes. Without UV irradiation, just like the P series, the N series of powders also did not provide any remarkable degradation, which indicates that all the further degradation upon UV will be caused by photocatalytic reaction only.

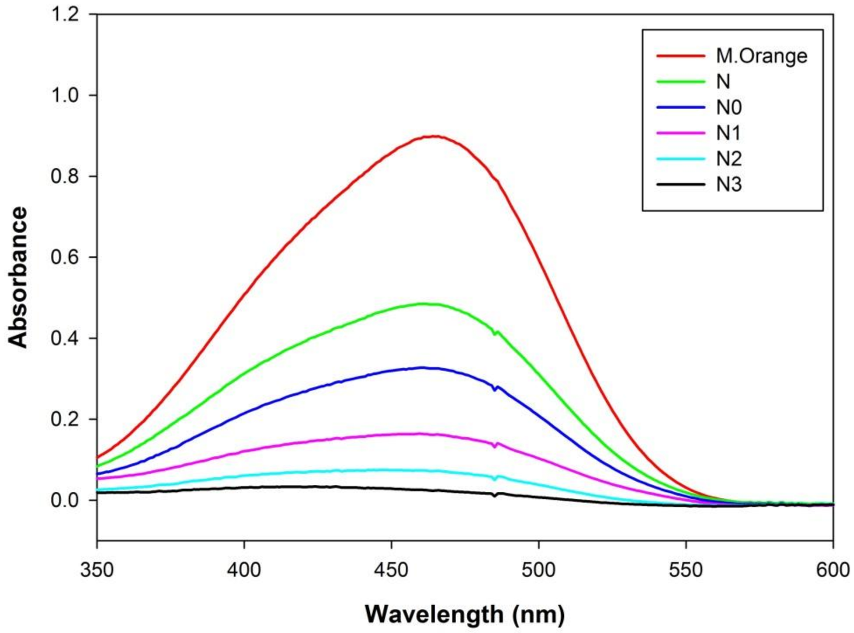

**Figure 4.3.3.** Absorbance spectra for the N series of powders.

As seen in Figure 4.3.3, the powders coded as N3 gave the best results in terms of the degradation of MO. Ball milling without Ag addition increased the photocatalytic activity implying that an increase on the specific surface area improves photocatalytic efficiency. Ag loading to this powder also improved the degradation of MO implying that photocatalytic efficiency of starting NT-22 powder increased when 0.49 wt% of Ag was loaded in it. As the Ag amount increases, amount of degradation of MO also keep on increasing. N3 powders decomposed 96.27% of MO in the MO solution in 60 min.

Values for the degradation of MO in the MO solution for the N series of powders are given in Table 4.3.2. Among the Ag loaded N series of powders, N3 showed better photocatalytic efficiency than N1 and N2 as shown in Figure 4.3.4. Results suggest that photocatalytic activity of the powder increases as the Ag loading is increased since Ag acts as electron traps to enhance the electron hole separation and transfer of trapped electron to the adsorbed $O_2$ (Sung-suh et al., 2004). This finding is an indication of and can be taken as the positive effect of Ag addition on photocatalytic properties.

**Table 4.3.2.** % MO Degradation of the N series of powders.

| | **%MO Degradation after** | | |
|---|---|---|---|
| **Powder** | 30 min (No UV) | 30 min (UV) | 60 min (UV) |
| N | 1.88 | 23.87 | 46.07 |
| N0 | 0.93 | 35.77 | 63.56 |
| N1 | 0.77 | 60.57 | 81.77 |
| N2 | 1.84 | 70.83 | 91.68 |
| N3 | 0.82 | 80.93 | 96.27 |

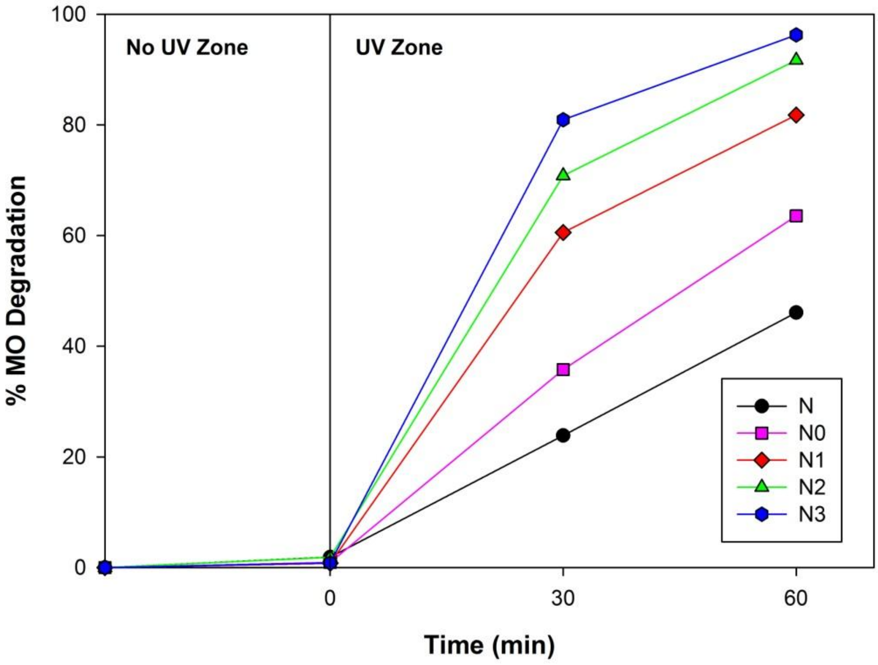

**Figure 4.3.4.** % MO Degradation for the N series of powders.

### 4.3.3.Photocatalytic Activity of the M series of Powders in MO Solution

The absorbance spectra obtained after 60 minutes of UV illumination for N series of powders are given in Figure 4.3.5. The absorbance spectra obtained after 60 min of UV illumination for the MO solution was included in the figure for comparison purposes. Just like the P and N series of powders, M series of powders did not provide any remarkable degradation without UV irradiation. That is an indication that all the further degradation upon UV will be caused by photocatalytic reaction only.

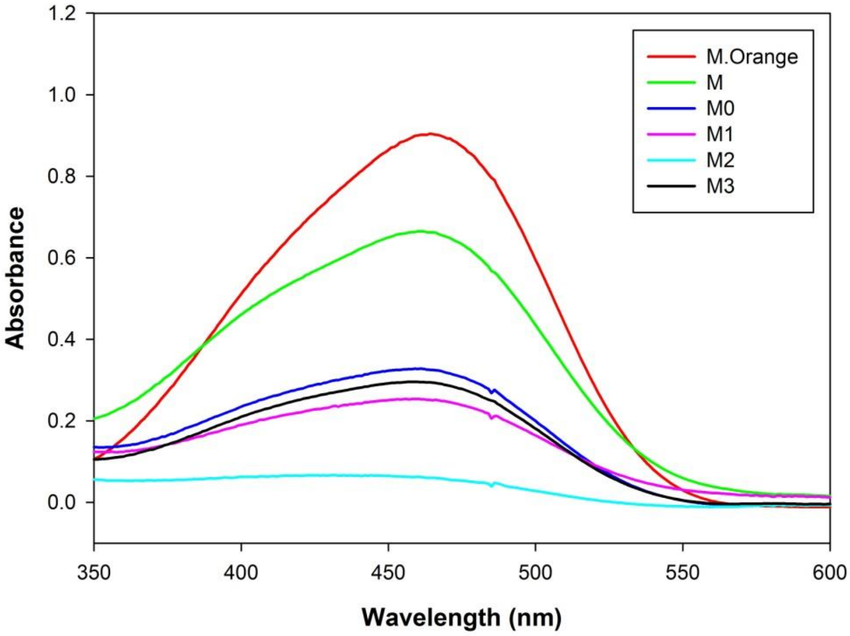

**Figure 4.3.5.** Absorbance spectra for M series of powders.

In the M series of powders, the starting $TiO(OH)_2$ powder gave the worst results in terms of the degradation of MO. Ball milling without Ag addition increased the photocatalytic activity, which can be attributed to the decrease in particle size and increase in specific surface area. Ag loading to $TiO(OH)_2$ powder improved the degradation of MO implying that photocatalytic efficiency of starting $TiO(OH)_2$ powder improved when 0.64 wt% of Ag was loaded in it. After Ag addition, photocatalytic activity of metatitanate powders increased significantly; however, it is also observed that high amount of Ag addition affected photocatalytic activity negatively implying that the optimal amount of Ag for this powders series was reached (Liu et al., 2003). It was stated in Section 2.3.2.1 that, Ag loading can decrease the photocatalytic activity especially excess amount of Ag is important since active $TiO_2$ sites can be blocked or light cannot access to $TiO_2$ due to Ag coverage. Moreover, recombination rates can be increased due to high amount of doping than optimal amount (Akgun et al., 2011a; Seery et al., 2007).

Values for the degradation of MO in the MO solution for the M series of powders are given in Table 4.3.3. Among the Ag loaded M series of powders, M2 showed better photocatalytic performance than M1 and M3 as shown in Figure 4.3.3. Results suggest that photocatalytic activity of the powder increases as the Ag loading is increased and excess amount of Ag can affect photocatalytic activity negatively.  This finding is an indication of and can be taken as the positive effect of Ag loading on photocatalytic properties.

**Table 4.3.3.** % MO Degradation of the M series of powders.

| | **%MO Degradation after** | | |
|---|---|---|---|
| **Powder** | 30 min (No UV) | 30 min (UV) | 60 min (UV) |
| M | 1.02 | 11.62 | 26.42 |
| M0 | 1.11 | 33.78 | 60.34 |
| M1 | 0.95 | 41.33 | 71.92 |
| M2 | 1.09 | 60.25 | 92.60 |
| M3 | 0.74 | 44.84 | 67.66 |

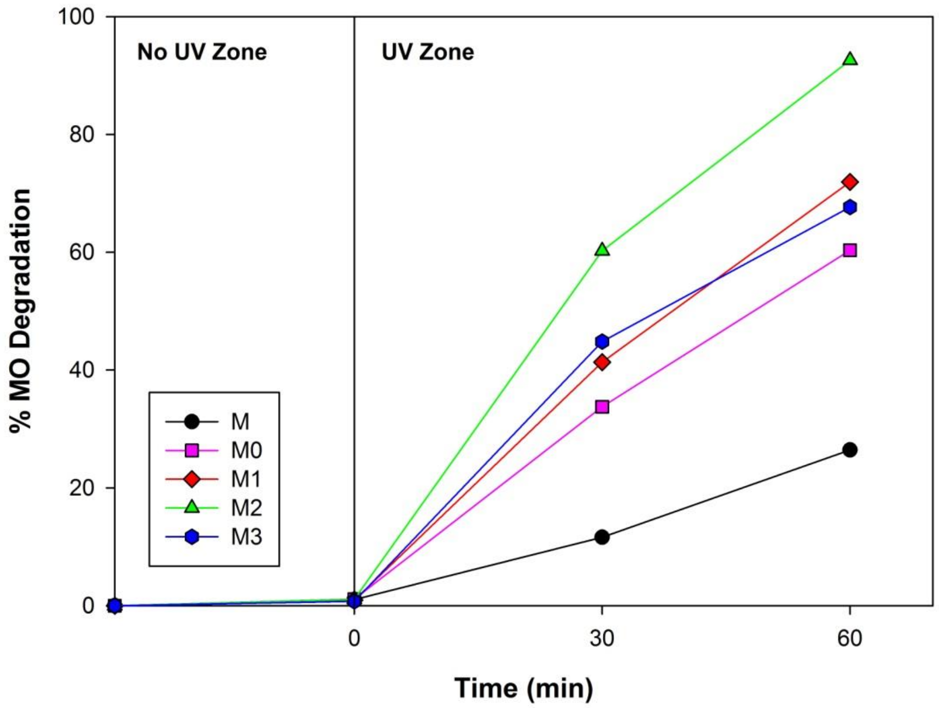

**Figure 4.3.6**. % MO Degradation for the M series of powders.

### 4.3.4. Mechanism for Photocatalytic Activity of Ag-Loaded $TiO_2$

When two materials having different work functions, such as $TiO_2$ and Ag, contact each other, formation of a Schottky barrier is observed. Electrons will be transferred from the material with low work function ($TiO_2$) to the material with high work function (Ag) which leads the electron transfer from $TiO_2$ and Ag. Those electrons transferred and loaded on the surface of Ag will be scavenged by the electron acceptor, commonly the oxygen molecules absorbed on the Ag surface. Moreover, some electrons transferred to Ag are contained in the body of $TiO_2$ and electron hole recombination rate is decreased by the transfer of electrons. Whether in body or on the surface of Ag, Ag atoms act as electron traps capturing certain amount of photoelectrons produced by UV excitation and this way, the separation between photoelectron and hole is increased (Hou et al., 2009). A schematic illustration of this mechanism is shown in Figure 4.3.7.

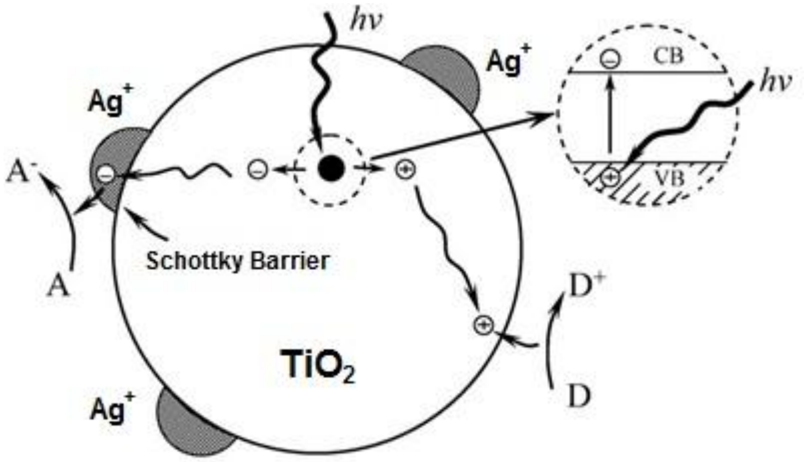

**Figure 4.3.7.** Schematic illustration of the photocatalysis mechanism of $TiO_2$ in the presence of Ag.

After ball milling of $AgNO_3$ added powders, Ag was detected as AgO form by XRD analysis. In principle UV illumination of $TiO_2$ can convert AgO to the native metal in the presence of $TiO_2$ (Page et al., 2007). AgO can be photodecomposed into O and Ag according to following reaction (Ohtani et al., 1993);

$$AgO \xrightarrow{\lambda} Ag + \frac{1}{2} O_2$$

Upon exposure of $TiO_2$ to UV, electron and holes are generated. AgO on $TiO_2$ is decomposed upon irradiation and forms Ag on the surface. This Ag can be generated to $Ag^+$ ion by holes and $Ag^+$ ion traps the electrons. The reaction mechanism of Ag added $TiO_2$ can be summarized as follows (Chen et al., 1994);

$$TiO_2 \xrightarrow{\lambda} e^-_{cb} + h^+_{vb}$$

The Ag on surface of $TiO_2$ can be generated to $Ag^+$ ions as;

$$Ag_s + h^+_{vb} \longrightarrow Ag^+_s$$

$$Ag^+_s + e^- \longrightarrow Ag_s$$

The photogenerated holes oxidized the preabsorbed $OH^-$ and $H_2O$ to generate HO free radical which reacts with adsorbed MO.

$$OH^-_s + h^+_{vb} \longrightarrow HO_s$$

$$H_2O_s + h^+_{vb} \longrightarrow HO_s + H^+$$

$$HO_s + MO \longrightarrow \text{colorless product}$$

The subscripts vb, cb, and s represent valence band, conductive band, and surface of catalyst, respectively.

## 4.4. WETTABILITY

Contact angle measurements on $TiO_2$ particle coated glass substrates were carried out to realize if Ag loading has any effect on hydrophilicity that is important for self cleaning applications. The powders having the best photocatalytic efficiency after Ag addition were chosen for wettability measurements. The wettability results of the Ag loaded powders were compared with the starting powders.

Contact angle measured by SEO Phoenix 300 for a bare (uncoated) glass substrate was 41°. Contact angle image for bare glass substrate is seen in Figure 4.4.1.

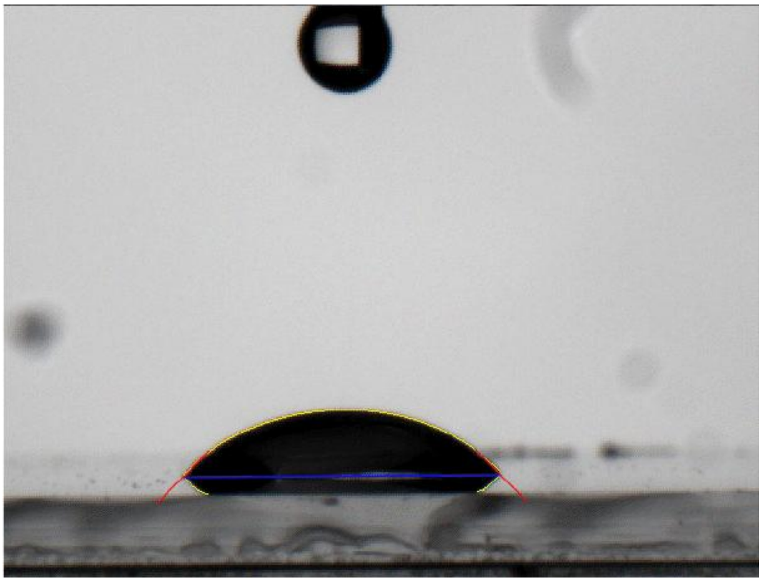

**Figure 4.4.1.** Contact angle image for bare glass substrate.

Contact angle images taken for the (a) P and (b) P3 powder coated glass substrate are shown in Figure 4.4.2. For both powder coated glass substrates contact angle was measured as 0° meaning that complete wetting was achieved.

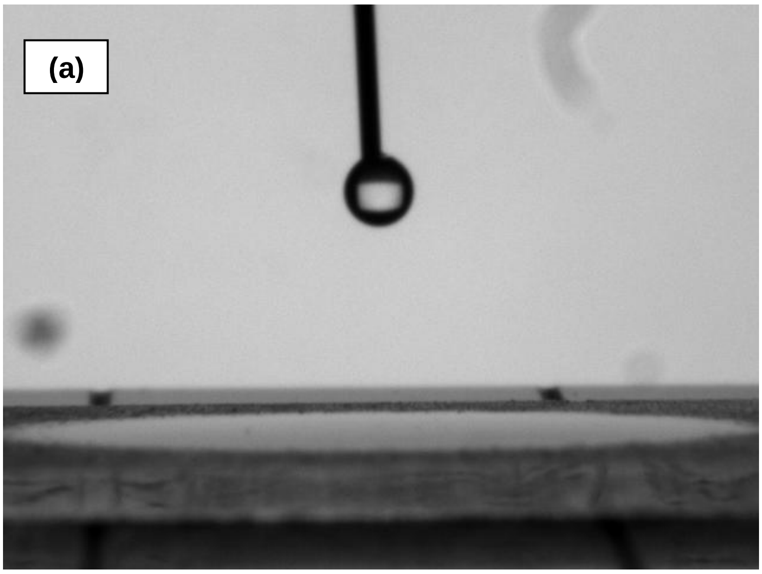

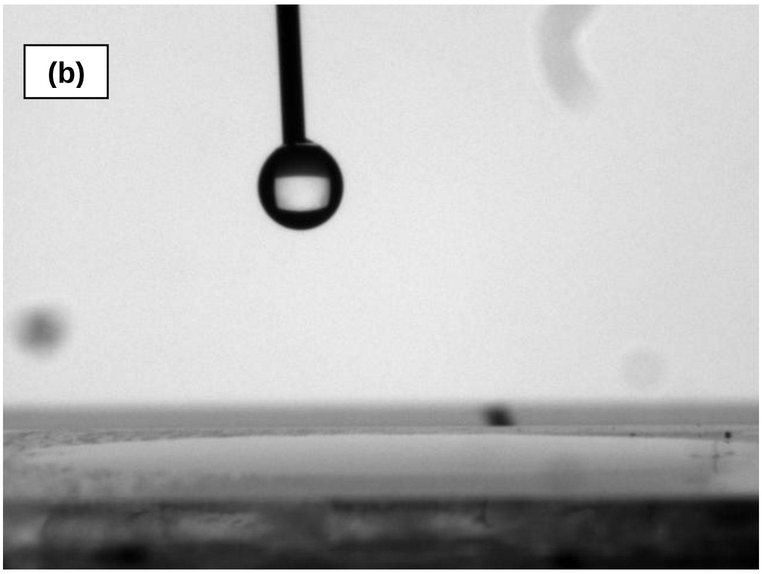

**Figure 4.4.2.** Contact angle images for **(a)** P and **(b)** P3 coated substrates.

P-25 has superior hydrophilic properties (Euvananont et al., 2008). As seen in Figure 4.4.2. it provides 100% wetting. After Ag loading to P-25, hydrophilic properties of P-25 were not worsened. 100% wetting was obtained also for the glass substrate coated by 1.88 wt% Ag containing $TiO_2$ powder.

Contact angle images taken for the (a) N and (b) N3 respectively powder coated glass substrates are shown in Figure 4.4.3. Contact angle for the N and N3 powder coated substrates were 23° and 5°, respectively.

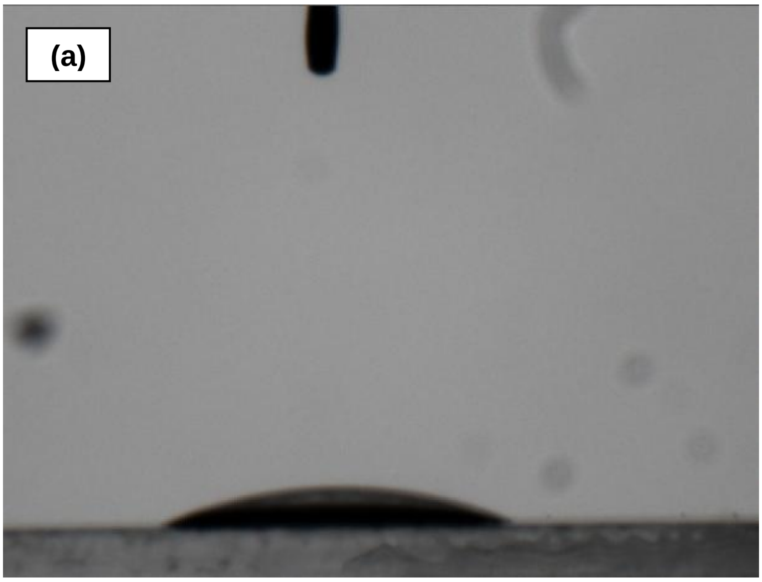

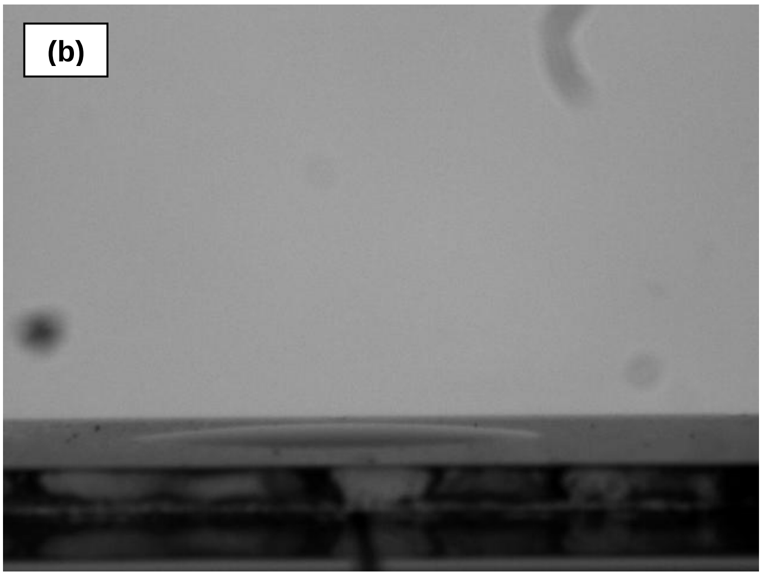

**Figure 4.4.3.** Contact angle image for **(a)** N and **(b)** N3 coated substrates.

It is known that, Ag addition decreases water contact angle by acceleration of $O_2$ formation, with the effect of decreasing recombination and increasing product yields initiated by h+ or OH (Meng and Fanming, 2009) and it is also believed that density of surface hydroxyl of the $TiO_2$ films is also related to hydrophilicity since hydroxyls can combine with water molecules to form hydrogen bond which results in good wettability (Euvananont et al., 2008).

Contact angle images taken for the M and M2 powder coated glass substrate are shown in Figure 4.4.4. Contact angle for the M and M2 powder coated substrates were 13° and 1°, respectively.

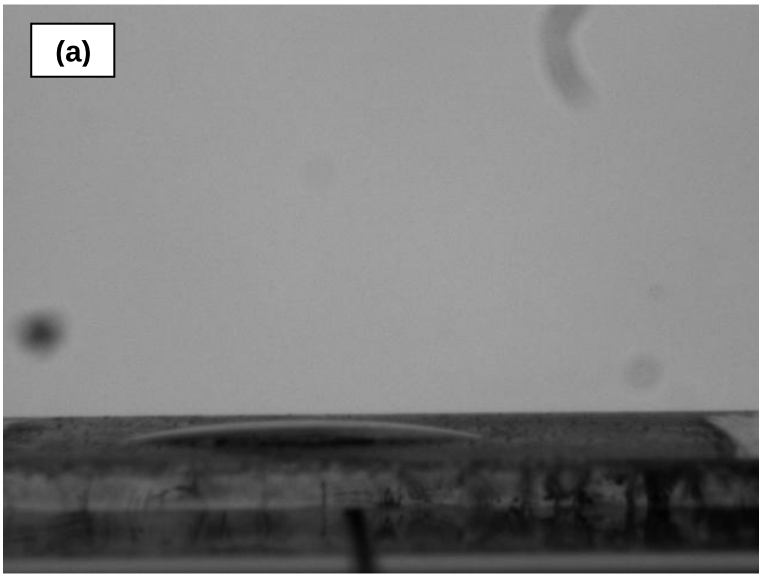

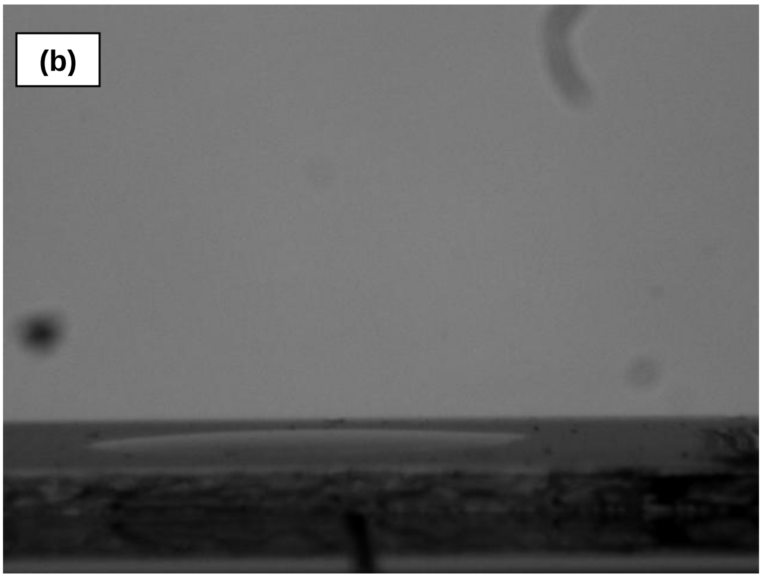

**Figure 4.4.4.** Contact angle images for **(a)** M and **(b)** M2 coated substrates.

Water contact angle was decreased via Ag addition by acceleration of $O_2$ formation, with the effect of decreasing recombination and increasing product yields initiated by h+ or OH (Meng and Fanming, 2009).

Glasses coated with Ag added $TiO_2$ have remarkable hydrophilic properties, contact angle measurements for selected powders are shown in Table 4.4.1.

**Table 4.4.1**. Contact angle measurements for selected powders.

| Powder | No Powder | P | P3 | N | N3 | M | M2 |
|---|---|---|---|---|---|---|---|
| Contact Angle | 41° | 0° | 0° | 23° | 5° | 13° | 1° |

## 4.5. ANTIBACTERIAL ACTIVITY

The photographs of substrates in agar plates with bacteria after waiting for 48 h at 37 °C are shown in Figure 4.5.1.

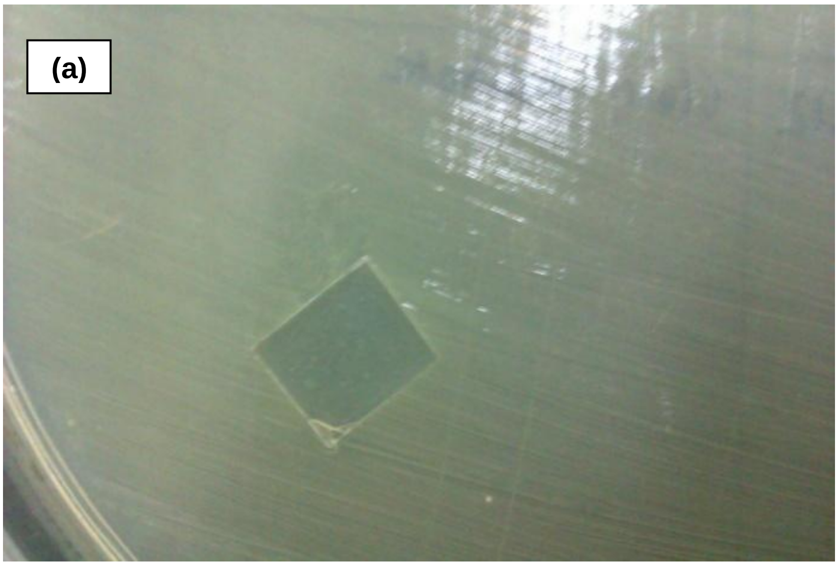

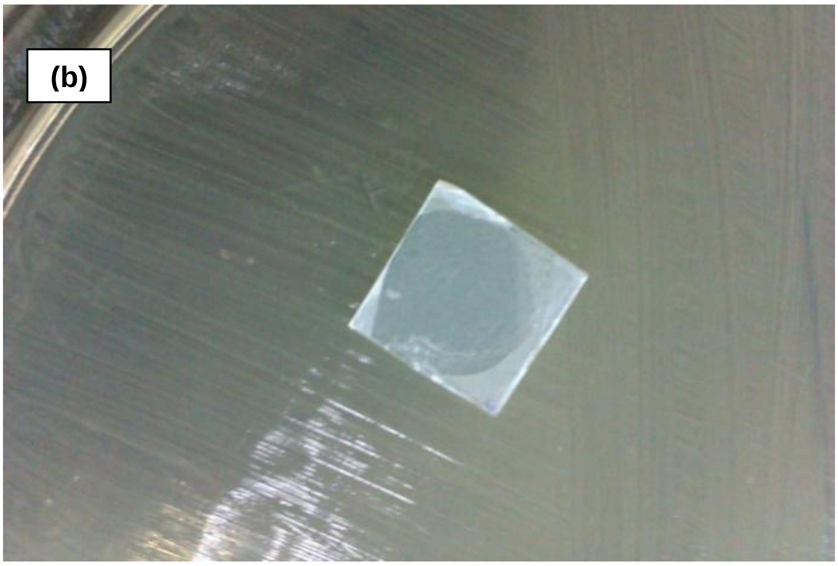
(b)

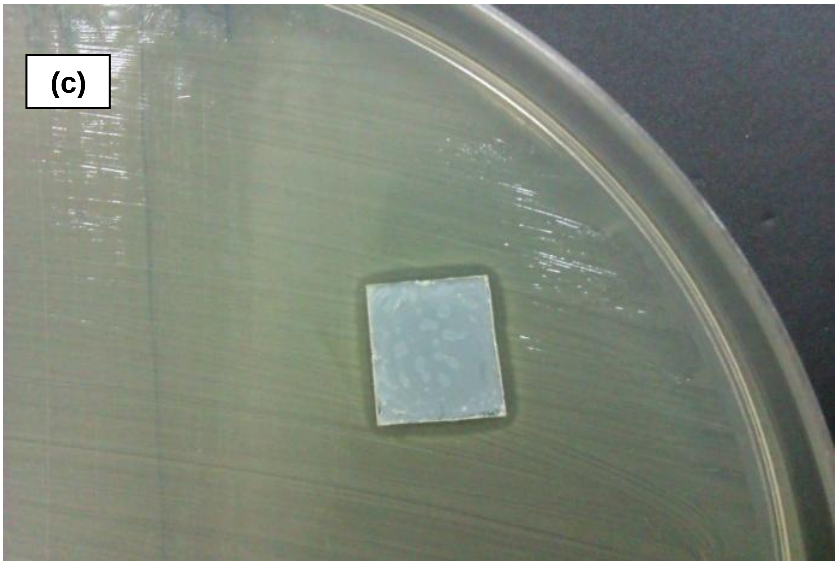
(c)

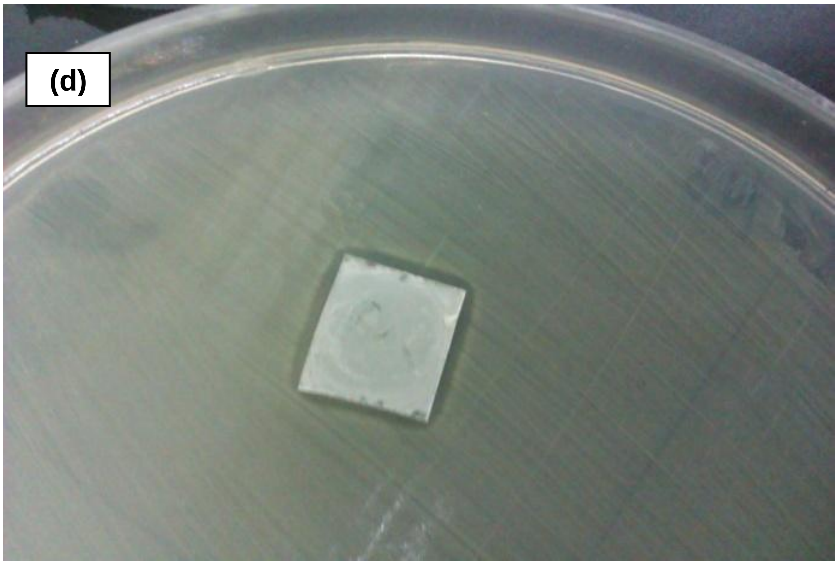

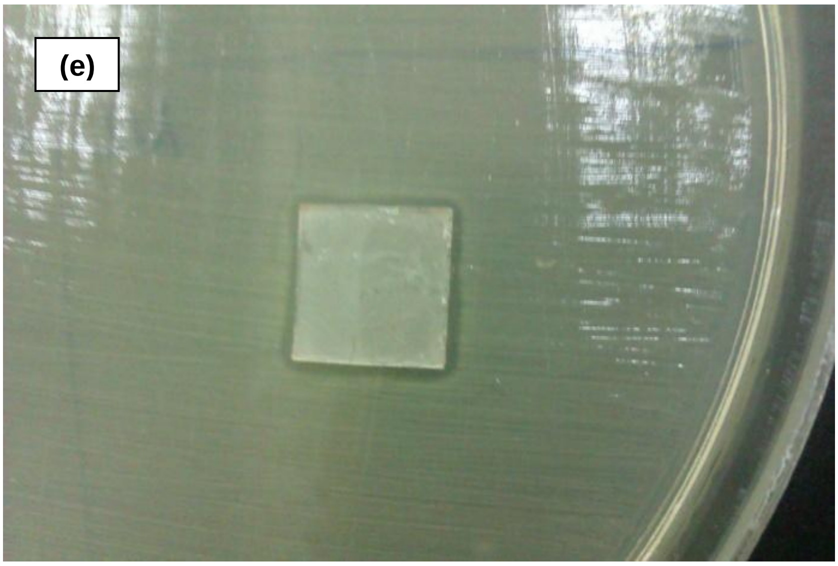

**Figure 4.5.1.** Photographs of glass substrates in agar plates with E.Coli. **(a)** No powder, **(b)** P, **(c)** P3, **(d)** N3 and **(e)** M2.

Bare glass substrate and P-25 coated substrates did not show any antibacterial activity. When the substrates with Ag added $TiO_2$ are examined, an opening around the glass substrate is observed. This clean area is the inhibition zone which can be defined as the bacterial free zone where the growth of bacteria is prevented. The presence of inhibition zone is an indicator of antibacterial activity (Akgun et al., 2011b). The antibacterial mechanism basically depends on the attack to the cell membrane of bacteria (Keleher et al., 2002). Hydroxyl radical formed upon UV irradiation of $TiO_2$ therefore provides antibacterial activity since these radicals effectively attack to cell membrane and breakdown the bacteria (Akgun et al., 2011b). In case of Ag, $Ag^+$ ions are the attacking mechanisms, but it is noted that Ag in the oxide form shows antibacterial activity whether a light source is present or not while $Ag^+$ does not have any activity if the light is absent (Page et al., 2007). The size measurement of inhibition zone can provide a comparison between powders antibacterial properties. However, for this case the zones formed were small in size and did not lead any comparative result. Since the aim of this measurement is beyond the scope of this study, no measurements were attempted and visual observation was considered as satisfactory.

# CHAPTER 5

# CONCLUSIONS

An investigation of the photocatalytic properties of Ag loaded $TiO_2$ powders produced by mechanical ball milling has led to the following conclusions.

1. Ag could be successfully loaded to $TiO_2$ powders by employing a planetary ball mill.
2. Ball milling exhibits a profound influence on the surface properties and photocatalytic activity of $TiO_2$ powders.
3. Powder characteristics and Ag loading have a profound influence on the photocatalytic properties of $TiO_2$ powders.
    a. For the P series of powders, a continuous improvement on photocatalytic activity by Ag loading observed, however due to ball milling, surface properties deteriorated which lowered photocatalytic activity.
    b. For the N series of powders, a direct relation between the photocatalytic activity and Ag loading was obtained. Ag loading and ball milling both improved photocatalytic activity.
    c. For the M series of powders, Ag loading and ball milling both improved photocatalytic activity. However, excess amount of Ag loading caused a decrease in photocatalytic activity.

4. Hydrophilic properties of $TiO_2$ enhanced after Ag loading. $TiO_2$ powders with best photocatalytic activity also exhibited enhanced wetting properties after Ag loading by ball milling.
5. $TiO_2$ powders could gain antibacterial prospect even without UV irradiation if Ag is loaded.
6. Ag loaded $TiO_2$ powders could be used effectively for photocatalytic and antibacterial applications which cannot reach any light source such as antibacterial sanitary wares or household applications.

# REFERENCES

- Akgun, B. A., Durucan, C., & Mellott, N. P. (2011a). Effect of silver incorporation on crystallization and microstructural properties of sol–gel derived titania thin films on glass. *Journal of Sol-Gel Science and Technology, 58*, 277-289.
- Akgun, B. A., Wren, A. W., Durucan, C., Towler, M. R., & Mellott, N. P. (2011b). Sol–gel derived silver-incorporated titania thin films on glass: bactericidal and photocatalytic activity. *Journal of Sol-Gel Science and Technology, 59*, 228-238.
- Algarin, P. C. (2008). *Effects of Zn doping and high energy ball milling on the photocatalytic properties of* $TiO_2$. Unpublished master's thesis, University of South Florida, Florida, USA.
- Arabatzis, I. M., Stergiopoulos, T., Bernard, M. C., Labou, D., Neophytides, S. G., & Falaras, P. (2003). Silver-modified titanium dioxide thin films for efficient photodegradation of methyl orange. *Applied Catalysis B: Environmental, 42,* 187-201.
- Bao, X.-wang, Yan, S.-S., Chen, F., & Zhang, J.-long. (2005). Preparation of $TiO_2$ photocatalyst by hydrothermal method from aqueous peroxotitanium acid gel. *Materials Letters, 59,* 412-415.
- Begin-Colin, S., Girot, T., Caer, G. L., & Mocellin, A. (2000). Kinetics and Mechanisms of Phase Transformations Induced by Ball-Milling in Anatase TiO2. Ournal of Solid State Chemistry, 149, 41-48.
- Bowering, N., Croston, D., Harrison, P. G., & Walker, G. S. (2007). Silver Modified Degussa P25 for the Photocatalytic Removal of Nitric Oxide. *International Journal of Photoenergy, 2007*, 1-8.
- Byrne, J. A., Fernandez-Ibañez, P. A., Dunlop, P. S. M., Alrousan, D. M. A., & Hamilton, J. W. J. (2011). Photocatalytic Enhancement for Solar Disinfection of Water: A Review*. International Journal of Photoenergy, 2011*, 1-12.
- Castro, C. L. D., & Mitchell, B. S. (2002). Nanoparticles from Mechanical Attrition. In M-I. Baraton, *Synthesis, Functionalization*

*and Surface Treatment of Nanoparticles* (pp.1-15). American Scientific Publishers.

- Chen, L., & Chou, T.-chuan. (1994). Photodecolorization of Methyl Orange Using Silver Ion Modified $TiO_2$ as Photocatalyst. *Industrial & Engineering Chemistry Research*, *33*, 1436-1443.
- Chou, L.-H., Chung, I.-C., & Hsu, P.-Y. (2005). Silver particle dispersed silver oxide film: a dual function write once recording material. *Proceedings of SPIE,* 5643, 276-284.
- Colón, G., Maicu, M., Hidalgo, M. C., & Navío, J. A. (2006). Cu-doped $TiO_2$ systems with improved photocatalytic activity. *Applied Catalysis B: Environmental, 67*, 41-51.
- Di Paola, A., Addamo, M., Bellardita, M., Cazzanelli, E., & Palmisano, L. (2007). Preparation of photocatalytic brookite thin films. *Thin Solid Films, 515*, 3527-3529.
- Dutta, H., Sahu, P., Pradhan, S. K., & De, M. (2002). Microstructure characterization of polymorphic transformed ball-milled anatase $TiO_2$ by Rietveld method. *Materials Chemistry and Physics, 77*, 153-164.
- El Saliby, I., Erdei, L., Kyong, H., & Kim, J.-Ho. (2011). Development of visible light sensitive titania photocatalysts by combined nitrogen and silver doping. *Journal of Industrial and Engineering Chemistry, 17*, 358-363.
- Ersöz, İ. T. (2009*). Application of semi conductor films over glass / ceramic surfaces and their low temperature photocatalytic activity*. Unpublished master's thesis, Middle East Technical University, Ankara, Turkey.
- Euvananont, C., Junin, C., Inpor, K., Limthongkul, P., & Thanachayanont, C. (2008). $TiO_2$ optical coating layers for self-cleaning applications. *Ceramics International, 34,* 1067-1071.
- Fadhel, H. B., Frances, C., & Mamourian, A. (1999). Investigations on ultra-fine grinding of titanium dioxide in a stirred media mill. *Powder Technology, 105*, 362-373.

- Fernández-ibáñez, P., Malato, S., & Nieves, F. J. D. (1999). Relationship between $TiO_2$ particle size and reactor diameter in solar photoreactors efficiency. *Catalysis Today, 54*, 195-204.
- Fujishima, A, & Zhang, X. (2006). Titanium dioxide photocatalysis: present situation and future approaches. *Comptes Rendus Chimie, 9*, 750-760.
- Fujishima, A., Rao, T. N., & Tryk, D. A. (2000). Titanium dioxide photocatalysis*. Journal of Photochemistry and Photobiology C: Photochemistry Reviews, 1*, 1-21.
- Gadalla, A., Cae, L., Humbert, O., Thomas, F., Toma, L. F., Bertrand, G., Zahraa, O., et al. (2009). On the Origin of the Decay of the Photocatalytic Activity of $TiO_2$ Powders Ground at High Energy. *The Journal of Physical Chemistry C, 113,* 16589-16602.
- Gajovic, A., Stubicar, M., Ivanda, M., & Furic, K. (2001). Raman spectroscopy of ball-milled $TiO_2$. *Journal of Molecular Structure, 563-564,* 315-320.
- Ghanbary, F. & Jafarian, A. (2011). Preparation and Photocatalytic Properties of Silver Doped Titanium Dioxide Nanoparticles and Using Artificial Neural Network for Modeling Photocatalytic Activity*. Australian Journal of Basic and Applied Sciences, 5(11),* 2193-2202.
- Guettaï, N., & Ait Amar, H. (2005). Photocatalytic oxidation of methyl orange in presence of titanium dioxide in aqueous suspension. Part II: kinetics study. *Desalination, 185*, 439-448.
- Han, C.-hwan, Lee, H.-soo, & Han, S.-do. (2010). Synthesis of Nanocrystalline $TiO_2$ by Sol-Gel Combustion Hybrid Method and Its Application to Dye Solar Cells. *The Bulletin of Korean Chemical Society, 29(8)*, 1495-1498.
- Han, J., Hyun, D., Kim, S.-jae, & Sub, K. (2008). Synthesis and photocatalytic property of a mixture of anatase and rutile $TiO_2$ doped with Fe by mechanical alloying process. *Journal of Alloys and Compounds, 459*, 386-389.

- Heller, A. (1981). Conversion of Sunlight into Electrical Power and Photoassisted Electrolysis of Water in Photoelectrochemical. *Accounts of Chemical Research, 14*, 154-162.
- Herrmann, J.-M. (2006). Photocatalysis. In *Kirk-Othmer Encyclopedia of Chemical Technology* (pp.1-39). John Wiley & Sons, Inc
- Hoffmann, M. R., Martin, S. T., Choi, W., & Bahnemannt, D. W. (1995). Environmental Applications of Semiconductor Photocatalysis. *Chemical Reviews,* 95, 69-96.
- Hong, S., Lee, M.S., Hwang, H.-S., Lim, K.-T., Park, S.S., Ju, C.-S., & Lee, G.-D. (2003). Preparation of titanium dioxides in the W/C microemulsions and their photocatalytic activity. *Solar Energy Materials & Solar Cells, 80(2003),* 273-282.
- Hong, Y. C., Bang, C. U., Shin, D. H., & Uhm, H. S. (2005). Band gap narrowing of $TiO_2$ by nitrogen doping in atmospheric microwave plasma, *Chemical Physics Letters, 413*, 454-457.
- Hou, X., Huang, M., Wu, X., & Liu, A. (2009). Preparation and studies of photocatalytic silver-loaded $TiO_2$ films by hybrid sol–gel method. *Chemical Engineering Journal, 146*, 42-48.
- Hung, W.-C., Fu, S.-H., Tseng, J.-J., Chu, H., & Ko, T.-H. (2007). Study on photocatalytic degradation of gaseous dichloromethane using pure and iron ion-doped $TiO_2$ prepared by the sol-gel method. *Chemosphere, 66*, 2142-2151.
- Iliev, V., Tomova, D., Bilyarska, L., Eliyas, A., & Petrov, L. (2006). Photocatalytic properties of $TiO_2$ modified with platinum and silver nanoparticles in the degradation of oxalic acid in aqueous solution. *Applied Catalysis B: Environmental, 63*, 266-271.
- Inagaki, M., Nakawaza, Y., Hirano, M., Kobayashi, Y., & Toyoda, M. (2001). Preparation of stable anatase-type $TiO_2$ and its photocatalytic performance. *International Journal of Inorganic Materials, 3*, 809-811.
- Jacoby, W. A., Maness, P. C., Wolfrum, E. J., Blake, D. M., & Fennell, J. A. (1998). Mineralization of Bacterial Cell Mass on a

Photocatalytic Surface in Air. *Environmental Science & Technology, 32(17),* 2650-2653.

- Jang, H. D., Kim, S.-kil, & Kim, S.-jin. (2001). Effect of particle size and phase composition of titanium dioxide nanoparticles on the photocatalytic properties. *Journal of Nanoparticle Research, 3,* 141-147.
- Kato, S., Hirano, Y., Iwata, M., Sano, T., Takeuchi, K., & Matsuzawa, S. (2005). Photocatalytic degradation of gaseous sulfur compounds by silver-deposited titanium dioxide*. Applied Catalysis B: Environmental, 57,* 109-115.
- Keleher, J., Bashant, J., Heldt, N., Johnson, L., & Li, Y. (2002). Photo-catalytic preparation of silver-coated $TiO_2$ particles for antibacterial applications. *World Journal of Microbiology & Biotechnology, 18,* 133-139.
- Kim, D.H., Choi, D.-K., Kim, S.-J., & Lee, K. S. (2008). The effect of phase type on photocatalytic activity in transition metal doped $TiO_2$ nanoparticles. *Catalysis Communications, 9, 654-657.*
- Kim, D.H., Hong, H., Kim, S., Song, J., & Lee, K. (2004). Photocatalytic behaviors and structural characterization of nanocrystalline Fe-doped $TiO_2$ synthesized by mechanical alloying. *Journal of Alloys and Compounds, 375*, 259-264.
- Kim, D.H., Lee, K. S, Kim, Y.-S., Chung, Y.-C., Kim, S.-J. (2006). Photocatalytic Activity of Ni 8 wt%-Doped $TiO_2$ Photocatalyst Synthesized by Mechanical Alloying Under Visible Light. *Journal of the American Ceramic Society, 89(2),* 515-518.
- Kolen'ko, Y. V., Maximov, V. D., Garshev, A. V., Meskin, P. E., Oleynikov, N. N., & Churagulov, B. R. (2004). Hydrothermal synthesis of nanocrystalline and mesoporous titania from aqueous complex titanyl oxalate acid solutions. *Chemical Physics Letters, 388*, 411-415.
- Kondo, M. M., & Jardim, W. F. (1991). Photodegradation Of Chloroform and Urea Using Ag-Loaded Titanium Dioxide As Catalyst, *Water Research, 25(7),* 823-827.

- Konta, R., Ishii, T., Kato, H., & Kudo, A. (2004). Photocatalytic Activities of Noble Metal Ion Doped $SrTiO_3$ under Visible Light Irradiation. *The Journal of Physical Chemistry B, 108*, 8992-8995.
- Kubacka, A., Ferrer, M., Martínez-Arias, A., & Fernández-García, M. (2008). Ag promotion of $TiO_2$-anatase disinfection capability: Study of Escherichia coli inactivation. *Applied Catalysis B: Environmental*, 84, 87-93.
- Kumar, S. G., & Devi, L. G. (2011). Review on modified $TiO_2$ photocatalysis under UV/visible light: Selected results and related mechanisms on interfacial charge carrier transfer dynamics*. The Journal of Physical Chemistry A, 115*, 13211-13241.
- Lau, L. D., Rodriguez, R., Henery, S., Manuel, D., & Schwendiman, L. (1998). Photoreduction of Mercuric Salt Solutions at High pH. *Environmental Science & Technology, 32*, 670-675.
- Lee, W., Shen, H.-S., Dwight, K., & Wold, A. (1993). Effect of Silver on the Photocatalytic Activity of $TiO_2$. *Journal of Solid State Chemistry, 106*, 288-294.
- Li, B., Wang, X., Yan, M., & Li, L. (2002). Preparation and characterization of nano-$TiO_2$ powder, *Materials Chemistry and Physics, 78*, 184-188.
- Liga, M. V., Bryant, E. L., Colvin, V. L., & Li, Q. (2010). Virus inactivation by silver doped titanium dioxide nanoparticles for drinking water treatment. *Water Research, 45,* 535-544.
- Linsebigler, A. L., Lu, G., & Yates, J. T. (1995). Photocatalysis on $TiO_2$ Surfaces: Principles, Mechanisms, and Selected Results. *Chemical Reviews, 95(3),* 735-758.
- Liu, Y., Liu, C.-Y., Rong, Q.-H., & Zhang, Z. (2003). Characteristics of the silver-doped $TiO_2$ nanoparticles*. Applied Surface Science, 220*, 7-11.
- Lu, C.-hsin, Wu, W.-hong, & Kale, R. B. (2008). Microemulsion-mediated hydrothermal synthesis of photocatalytic $TiO_2$ powders*. Journal of Hazardous Materials, 154*, 649-654.

- Maurya, A., & Chauhan, P. (2011). Structural and optical characterization of CdS/$TiO_2$ nanocomposite. *Materials Characterization, 62*, 382-390.
- Meng, F., Sun, Z. (2009). A mechanism for enhanced hydrophilicity of silver nanoparticles modified $TiO_2$ thin films deposited by RF magnetron sputtering. *Applied Surface Science, 255*, 6715-6720.
- Mills, A., & Hunte, S. L. (2000). An overview of semiconductor photocatalysis. *Journal of Photochemistry and Photobiology A,: Chemistry, 108,* 1-35.
- Mio, H., Kano, J. & Saito, F. (2004). Scale-up method of planetary ball mill. *Chemical Engineering Science, 59,* 5909-5916.
- Nam, W. S., & Han, G. Y. (2003). A Photocatalytic Performance of $TiO_2$ Photocatalyst Prepared by the Hydrothermal Method. *Korean Journal of Chemical Engineering, 20(1),* 180-184.
- Niederberger, M. & Pinna, N. (2009). Aqueous and Nonaqueous Sol-Gel. In *Metal Oxide Nanoparticles in Organic Solvents: Synthesis, Formation, Assembly and Application* (pp. 7-18).
- Nolan, N. T. (2010). *Sol-Gel Synthesis and Characterisation of Novel Metal Oxide Nanomaterials for Photocatalytic Applications* Unpublished doctoral dissertation, Dublin Institute of Technology, Dublin, Ireland.
- Ohtani, B., Zhang, S.-W., Ogita, T. Nishimoto, S. & Kagiya, T. (1993). Photoactivation of silver loaded on titanium (IV) temperature decomposition of ozone. *Journal of Photochemistry and Photobiology A: Chemistry, 71*, 195-198.
- Ovenstone, J. (2001). Preparation of novel titania photocatalysts with high activity. *Journal of Materials Science, 36*, 1325 - 1329.
- Page, K., Palgrave, R. G., Parkin, I. P., Wilson, M., Savin, L. P., & Chadwick, A. V. (2007). Titania and silver – titania composite films on glass — potent antimicrobial coatings. *Journal of Materials Chemistry, 95*, 95-104.
- Park,H.S., Kim, D.H., Kim, S.J., & Lee, K.S. (2006). The photocatalytic activity of 2.5wt% Cu-doped $TiO_2$ nano powders

synthesized by mechanical alloying. *Journal of Alloys and Compounds, 415*, 51-55.

- Priya, R., Baiju, K. V., Shukla, S., Biju, S., Reddy, M. L. P., Patil, K., & Warrier, K. G. K. (2009). Comparing Ultraviolet and Chemical Reduction Techniques for Enhancing Photocatalytic Activity of Silver Oxide / Silver Deposited Nanocrystalline Anatase Titania. *The Journal of Physical Chemistry A, 113*, 6243-6255.
- Raj, K. J. A., & Viswanathan, B. (2009). Effect of surface area , pore volume and particle size of P25 titania on the phase transformation of anatase to rutile. *Indian Journal of Chemistry, 48(A),* 1378-1382.
- Rattanakam, R., & Supothina, S. (2009). Visible-light-sensitive N-doped $TiO_2$ photocatalysts prepared by a mechanochemical method: effect of a nitrogen source. *Research on Chemical Intermediates, 35*, 263-269.
- Sahoo, C., Gupta, A.K., & Pal, A. (2005). Photocatalytic degradation of Crystal Violet (C.I. Basic Violet 3) on silver ion doped $TiO_2$. *Dyes and Pigments, 66*, 189-196.
- Sakthivel, S., Shankar, M. V., Palanichamy, M., Arabindoo, B., Bahnemann, D. W., & Murugesan, V. (2004). Enhancement of photocatalytic activity by metal deposition: characterisation and photonic efficiency of Pt, Au and Pd deposited on $TiO_2$ catalyst. Water research, 38, 3001-3008.
- Salari, M., Mousavi, S. M., Marashi, P., & Rezaee, M. (2009). Synthesis of $TiO_2$ nanoparticles via a novel mechanochemical method*. Journal of Alloys and Compounds, 469*, 386-390.
- Scalafani, A., Palmisano, L., & Davi, E. (1991). Photocatalytic degradation of phenol in aqueous polycrystalline $TiO_2$ dispersions : the influence of $Fe3^+$ , $Fe2^+$ and $Ag^+$ on the reaction rate. *Journal of Photochemistry and Photobiology A: Chemistry, 56*, 113-123.
- Seery, M. K., George, R., Floris, P., & Pillai, S. C. (2007). Silver doped titanium dioxide nanomaterials for enhanced visible light photocatalysis. *Journal of Photochemistry and Photobiology A: Chemistry, 189*, 258-263.

- Shifu, C., Wei, Z., Wei, L., & Sujuan, Z. (2008). Preparation , characterization and activity evaluation of p – n junction photocatalyst p-ZnO/n-$TiO_2$. *Applied Surface Science, 255,* 2478-2484.
- Sobana, N., Muruganadham, M., & Swaminathan, M. (2006). Nano-Ag particles doped $TiO_2$ for efficient photodegradation of Direct azo dyes. *Journal of Molecular Catalysis A: Chemical, 258,* 124-132
- Sonawane, R. S., Hegde, S.G ., & Dongare, M.K . (2003). Preparation of titanium(IV) oxide thin film photocatalyst by sol–gel dip coating. *Materials Chemistry and Physics, 77*, 744-750.
- Sondi, I., Goia, D. V., & Matijevi, E. (2003). Preparation of highly concentrated stable dispersions of uniform ssilver nanoparticles. Journal of Colloid and Interface Science, 260, 75-81.
- Su, C., Hong, B., & Tseng, C. (2004). Sol – gel preparation and photocatalysis of titanium dioxide, *Catalysis Today, 96,* 119-126.
- Sun, B., & Smirniotis, P. G. (2003). Interaction of anatase and rutile $TiO_2$ particles in aqueous photooxidation. *Catalysis Today, 88,* 49-59.
- Sun, J., Gao, L., & Zhang, Q. (2003). Synthesizing and Comparing the Photocatalytic Properties of High Surface Area Rutile and Anatase Titania Nanoparticles. *Journal of the American Ceramic Society, 86(10)*, 1677-1682.
- Sung-suh, H. M., Choi, J. R., Hah, H. J., Koo, S. M., & Bae, Y. C. (2004). Comparison of Ag deposition effects on the photocatalytic activity of nanoparticulate $TiO_2$ under visible and UV light irradiation. *Journal of Photochemistry and Photobiology A: Chemistry, 163*, 37-44.
- Takahashi, A., Hamakawa, N., Nakamura, I., & Fujitani, T. (2005). Effects of added 3d transition-metals on Ag-based catalysts for direct epoxidation of propylene by oxygen. *Applied Catalysis A: General, 294,* 34-39.

- Taoda, H. (2008). Development of $TiO_2$ photocatalysts suitable for practical use and their applications in environmental cleanup. *Research on Chemical Intermediates, 34(4*), 417- 426.
- Tayade, R. J., Kulkarni, R. G., & Jasra, R. V. (2006). Transition Metal Ion Impregnated Mesoporous $TiO_2$ for Photocatalytic Degradation of Organic Contaminants in Water. *Industrial & Engineering Chemistry Research, 45*, 5231-5238.
- Thompson, T. L., & Yates, J. T. (2006). Surface Science Studies of the Photoactivation of $TiO_2$ - New Photochemical Processes. *Chemical Reviews, 106*, 4428-4453.
- Tong, T., Zhang, J., Tian, B., Chen, F., & He, D. (2008). Preparation of $Fe^{3+}$-doped $TiO_2$ catalysts by controlled hydrolysis of titanium alkoxide and study on their photocatalytic activity for methyl orange degradation. *Journal of Hazardous Materials, 155*, 572-579.
- Tryba, B., Piszcz, M., & Morawski, A. W. (2010). Photocatalytic and Self-Cleaning Properties of Ag-Doped $TiO_2$.*The Open Materials Science Journal, 4*, 5-8.
- Wang, Xuefei, Li, S., Yu, H., Yu, J., & Liu, S. (2011). $Ag_2O$ as a new visible-light photocatalyst: self-stability and high photocatalytic activity. *Chemistry - A European Journal, 17,* 7777-7780.
- Wang, Y., Cheng, H., Hao, Y., Ma, J., Li, W., & Cai, S. (1999). Preparation , characterization and photoelectrochemical behaviors of Fe (III) -doped $TiO_2$ nanoparticles.*Journal of Materials Science, 34*, 3721-3729.
- Whang, T.-jen, Huang, H.-yu, Hsieh, M.-tao, & Chen, J.-jen. (2009). Laser-Induced Silver Nanoparticles on Titanium Oxide for Photocatalytic Degradation of Methylene Blue. *International Journal of Molecular Sciences, 10*, 4707-4718.
- Wodka, D., Bielanska, E., Socha, R.P., Nowak, P. & Warszynski, P. (2010). Influence Of The Decomposed Substrates on the Photocatalytic Activity of the Titanium Dioxide Modified by Silver Nanoparticles. *Physicochemical Problems of Mineral Processing, 45*, 99-112.

- Woo, S. H., Kim, W. W., Kim, S. J., & Rhee, C. K. (2007). Photocatalytic behaviors of transition metal ion doped $TiO_2$ powder synthesized by mechanical alloying. *Materials Science and Engineering: A, 449-451*, 1151-1154.
- Wu, P., Xie, R., Imlay, K., & Shang, J. K. (2010). Visible-light-induced bactericidal activity of titanium dioxide codoped with nitrogen and silver*. Environmental Science & Technology, 44,* 6992-7007.
- Xie,J., Lü,X., Liu, J., & Shu, H. (2009). Brookite titania photocatalytic nanomaterials: Synthesis, properties, and applications*. Pure and Applied Chemistry, 81(12*), 2407-2415.
- Xin, B., Jing, L., Ren, Z., Wang, B., & Fu, H. (2005). Effects of Simultaneously Doped and Deposited Ag on the Photocatalytic Activity and Surface States of $TiO_2$. *The Journal of Physical Chemistry B, 109,* 2805-2809.
- Yin, S., Komatsu, M., Zhang, Q., Saito, F., & Sato, T. (2007). Synthesis of visible-light responsive nitrogen/carbon doped titania photocatalyst by mechanochemical doping. *Journal of Materials Science, 42(7),* 2399-2404.
- Yin, S., Komatsu, M., Zhang, Q., Saito, F., & Sato, T. (2006). Mechanochemical Synthesis of Visible-light Induced Photocatalyst with Nitrogen and Carbon Doping. *The Chinese Journal of Process Engineering, 6(3),* 3-7.
- Yin, S., Yamaki, H., Komatsu, M., Zhang, Q., Wang, J., Tang, Q., Saito, F., & Sato, T (2003). Preparation of nitrogen-doped titania with high visible light induced photocatalytic activity by mechanochemical reaction of titania and hexamethylenetetramine. *Journal of Materials Chemistry, 13*, 2996-3001.
- Zaleska, A. (2008). Doped-$TiO_2$: A Review*. Recent Patents on Engineering, 2*, 157-164.
- Zhang,F.L., Zhu, M., & Wang, C. Y. (2008). Parameters optimization in the planetary ball milling of nanostructured tungsten carbide /

cobalt powder. *International Journal of Refractory Metals & Hard Materials, 26,* 329-333.

- Zhang, Z., Wang, C.-chi, Zakaria, R., & Ying, J. Y. (1998). Role of Particle Size in Nanocrystalline $TiO_2$ -Based Photocatalysts. The Journal of Physical Chemistry B, 102, 10871-10878.
- Zhou, M., Yu, J., & Cheng, B. (2006). Effects of Fe-doping on the photocatalytic activity of mesoporous $TiO_2$ powders prepared by an ultrasonic method. *Journal of Hazardous Materials B, 137*, 1838-1847.
- Zhou, Z., Zhang, X., Wu, Z. & Dong, L. (2005). Mechanochemical preparation of sulfur-doped nanosized $TiO_2$ and its photocatalytic activity under visible light. *Chinese Science Bulletin, 50(23),* 2691-2695.
- Zhu, J., Zheng, W., He, B., Zhang, J. & Anpo, M. (2004). Characterization of Fe–$TiO_2$ photocatalysts synthesized by hydrothermal method and their photocatalytic reactivity for photodegradation of XRG dye diluted in water*. Journal of Molecular Catalysis A: Chemical, 216,* 35-43.